Liquid–liquid phase separation in solutions of ionic liquids: phase diagrams, corresponding state analysis and comparison with simulations of the primitive model

2009 J. Phys.: Condens. Matter 21 424119

(http://iopscience.iop.org/0953-8984/21/42/424119)

J. Phys.: Condens. Matter **21** (2009) 424119 (21pp) doi:10.1088/0953-8984/21/42/424119

Liquid–liquid phase separation in solutions of ionic liquids: phase diagrams, corresponding state analysis and comparison with simulations of the primitive model

W Schröer[1] **and V R Vale**

Institut für Anorganische und Physikalische Chemie, Fachbereich Biologie-Chemie, Universität Bremen, D-28359 Bremen, Germany

E-mail: schroer@uni-bremen.de

Received 2 June 2009
Published 29 September 2009
Online at stacks.iop.org/JPhysCM/21/424119

Abstract

Phase diagrams of ionic solutions of the ionic liquid $C_{18}mim^{+}NTF_2^{-}$ (1-n-octadecyl-3-methyl imidazolium bistrifluormethylsulfonylimide) in decalin, cyclohexane and methylcyclohexane are reported and compared with that of solutions of other imidazolium ionic liquids with the anions NTF_2^{-}, Cl^{-} and $BF4^{-}$ in arenes, CCl_4, alcohols and water. The phase diagrams are analysed presuming Ising criticality and taking into account the asymmetry of the phase diagrams. The resulting parameters are compared with simulation results for equal-sized charged hard spheres in a dielectric continuum, the restricted primitive model (RPM) and the primitive model (PM) that allows for ions of different size. In the RPM temperature scale the critical temperatures vary almost linearly with the dielectric permittivity of the solvent. The RPM critical temperatures of the solutions in non-polar solvents are very similar, somewhat below the RPM value. Correlations with the boiling temperatures of the solvents and a dependence on the length of the side chain of the imidazolium cations show that dispersion interactions modify the phase transition, which is mainly determined by Coulomb forces. Critical concentrations, widths of the phase diagrams and the slopes of the diameter are different for the solutions in protic and aprotic solvents. The phase diagrams of the solutions in alcohols and water get a lower critical solution point when represented in RPM variables.

1. Introduction

Studies of phase diagrams of ionic fluids are of fundamental interest, because the phase transitions can be expected to be driven or strongly influenced by the Coulomb interactions. As a consequence of the long-range nature of the Coulomb interactions it was hypothesized that the nature of the critical point of the phase transition in ionic fluids may be different [1–3] from the universal 3d Ising criticality, which is generally expected and observed for liquid–gas and liquid–liquid phase transitions in three dimensions driven by short-range r^{-n} interactions, where $n > 4.97$ [4, 5]. We recall that classical mean-field theories such as the van der Waals theory or the regular solution theory and their various generalizations predict parabolic temperature dependence for coexistence curves, while the 3d Ising model predicts a nearly cubic shape, in agreement with experiments [4–6]. Likewise the temperature dependence of other properties such as the susceptibility, the correlation length of the critical fluctuations and specific heat observed in non-ionic fluids agree with the properties of the 3d Ising model but not with any mean-field theory.

Mean-field critical behaviour was discussed as a possibility for phase transitions in ionic fluids [1–3] because of the long-range nature of the Coulomb interactions. In

[1] Author to whom any correspondence should be addressed.

fact, mean-field behaviour was reported for the coexistence curve of the liquid–vapour transition of the salt NH_4Cl [7], observed at 1150 K. In view of the rather limited accuracy of the very demanding high temperature measurements Pitzer suggested investigating liquid–liquid phase transitions of ionic solutions [1], because the phase transitions in ionic solutions driven by Coulomb interactions are expected to belong to the same universality class as the liquid–vapour transition of pure salts according to the correspondence principle [4]. First measurements of the coexistence curve [8] and of the critical opalescence [9] of an ionic solution in a solvent of low dielectric permittivity yielded indeed mean-field criticality, apparently corroborating the hypothesis of mean-field criticality. However, later work could not state those reports [10] and indicated possible errors in the measurements [11, 12]. Ensuring equilibration of the samples Ising criticality was consistently observed in subsequent investigations of the viscosity [13–16], of the phase diagrams [10, 17–19] and in light scattering investigations of the critical fluctuations [10, 12, 20–23] of the liquid–liquid phase transition of ionic solutions. Experiments on ionic solutions with ions differing in the charge of the ions [24] are also consistent with Ising criticality. According to the experiments it is now almost certain that liquid–liquid phase transitions in ionic solutions belong to the 3d Ising universality class. One might even reverse the argument and expect some shortcomings in the measurements, when Ising behaviour is not found [12]. Nevertheless, some doubts may remain because chemical instability is a major topic of all systems investigated experimentally until now. The solution of $N_{2226}B_{2226}$ (triethyl-hexylammonium triethyl-hexylborate) in biphenylether, which was proposed by Pitzer and investigated in [8–11], changes the critical temperature with time [11]. Furthermore different batches of the salt yield rather different figures for the critical temperature. The picrates used in [14, 15, 17, 25–27] are explosives. Therefore, investigations on the criticality of ionic solutions using stable and pure compounds are still of interest.

Comparison of critical properties with simulations is by no means a straightforward task. Simulations of critical properties are most demanding because they require the application of finite size scaling (FSS) techniques. Therefore simulations of critical properties are possible only for very simple model fluids at present. Simulations of the critical properties of ionic solutions are not yet available. The simple models of ionic fluids, which have been investigated, are the restricted primitive model (RPM) [28–30], which consists in equal-sized charged hard spheres in a dielectric continuum, and the more general primitive model (PM) that allows for ions differing in size [31, 32] and also charge [33–35]. For a review on simulations see [36]. Simulations of the RPM and the PM yield indeed Ising critical behaviour. Identifying the dielectric permittivity in the RPM with that of the solvent, the RPM may be taken as a cartoon of a real ionic solution. The critical properties of the liquid–gas phase transition of the model can be expected to apply also for the liquid–liquid phase transition. Thus, the experimental observation of Ising criticality for the liquid–liquid phase transition of ionic solutions is in agreement with the simulation results of the model systems.

Theory describing the criticality of ionic systems correctly is not available until now. At the mean-field level, however, theories have been developed, which compare well with the results of earlier simulation [37–39] which did not use finite size scaling techniques and may be regarded as 'mean-field' simulations. The simplest of these theories for the RPM is the Debye–Hückel (DH) theory [40] which accounts for electrostatic interactions among the ions. An extension of this early theory of ionic fluids was developed by Fisher and Levin [41, 42]; their theory predicts a coexistence curve which agrees rather well with the results of early simulations [37–39]. The Fisher–Levin (FL) theory goes beyond the original DH theory for strong electrolytes by incorporating ion pairing (following the ideas of Bjerrum) and accounting for the interactions of free ions and ion pairs by macroscopic electrostatics as the DH theory does for ion–ion interactions. According to the nature of mean-field theories, the critical temperature is overestimated and the critical density is underestimated if compared to the results of simulations employing finite size scaling. Nevertheless, the critical data are located in the correct region of the temperature–density plane by the FL theory, while the original DH theory, which yields a rather good figure for the critical temperature of the RPM [2, 43], underestimates the critical density by an order of magnitude. The agreement of the FL theory and of its generalization to charge asymmetric fluids [44] with the simulations is better than that of theories that are based on cluster expansions [3] and appear to be more advanced from the statistical mechanical point of view.

The FL theory explains the fact that, in spite of the long-range nature of the Coulomb interactions, mean-field criticality is not observed: Ising criticality in an ionic system appears as a consequence of the shielding of the Coulomb interactions by the charge distribution surrounding an ion, so that the correlations become effectively short range and Ising criticality may result.

A very demanding problem for theory, simulation and experiments in the field of critical phenomena is the crossover from mean-field criticality to Ising criticality when approaching the critical temperature. The transition from Ising to mean-field criticality can be described by a crossover theory [44]. The Ginzburg temperature marks the range of applicability of a mean-field theory. Estimates of the Ginzburg temperature of the RPM based on the Fisher–Levine theory predict a crossover from Ising to mean-field criticality that is further apart from the critical point than expected for non-ionic fluids, thus excluding the possibility of mean-field behaviour for the RPM [46–48]. Other theories yield the opposite prediction [49, 50]. The prediction of a large Ginzburg temperature is at variance with experimental observations [51]. Therefore, decisive experiments of critical properties in a large temperature range and their analysis in terms of a crossover theory [45, 52] remain a challenging topic. Such experiments are rather difficult, because they require experiments in a large temperature range. The necessary scattering experiments must include regions with small scattering intensity and require measurements of phase diagrams in regions where non-universal specific properties become important so that

the analysis of the data at large separation from the critical temperature may become inconclusive.

A further fundamental property of the phase diagrams is the diameter of the coexistence curves that describes the temperature dependence of the mean of the compositions of the two coexisting phases. For long time linearity of this curve was assumed, which is known as the rectilinear diameter rule of Cailletet–Mathias. It is now well established that the rectilinear diameter rule is incorrect and non-analytic contributions determine the behaviour, when approaching the critical point [53]. The relative importance of the various non-analytic terms determining the asymptotic behaviour is difficult to assess and remains an actual topic of experimental and theoretical investigations [54–57].

Chemical pure and stable systems are the conditions for good experiments that clarify such settled problems as the crossover or the asymmetry of the phase diagrams. Unfortunately the very stable solutions of typical inorganic salts such as NaCl are not appropriate. Liquid–liquid phase transitions are not observed at ambient conditions in such solutions, because crystallization occurs already at higher temperatures than may be expected for a liquid–liquid phase transition. For solutions of inorganic salts homogeneous solutions or limited solubility determined by the equilibrium between the solution and the crystalline solid salt are commonly found. Investigations in solutions in non-polar solvents are not possible, because the solubility of the typical inorganic salts decreases, if water is replaced by less polar solvents, so that the solubility of salts in hydrocarbons is extremely low.

Only solutions of salts with low melting points can be expected to show a liquid–liquid phase transition at ambient conditions. However, chemical stability is an issue for the organic salts considered in the investigations before 2000 [9–27]. For reviews of this work see [57–60]. A new group of salts with melting points below 100 °C, termed ionic liquids (IL), became recently available in good quality. In view of their many applications ILs have become major topics of research in chemistry, physics and chemical engineering [61–63]. The special properties of the ILs suggest many applications, e.g. as reaction medium, catalyst and extraction medium. ILs are organic salts with at least one largish non-spherical ion. Some ILs have melting points at temperatures as low as −70 °C [64]. The vapour pressure of ILs is hardly measurable [65]. Boiling temperatures are expected near 1300 K [66], which is far above the decomposition temperatures near 600 K [67].

The properties of the ILs are founded in the interplay of Coulomb interactions and other interactions of the ions [68]. Thus solutions of ILs in polar, and non-polar solvents are possible and quite a few systems with a critical point of the liquid–liquid phase transition at ambient temperatures have been discovered recently [69–81]. Systematic studies of the liquid–liquid phase transition of ILs in solutions are important for applications in separation techniques and help clarify the relations between the molecular and the thermodynamic properties of the solutions.

In view of the large number of new systems it is necessary to get a comprehensive overview. A powerful tool for reducing the data and to pin-point general aspects of the systems under consideration is the concept of corresponding states [6]. The theorem of corresponding states, which goes back to van der Waals, predicts that scaling the thermodynamic variables with their critical data leads to a universal representation of the thermodynamic properties, e.g. of the phase diagrams. The phase diagrams match on a master curve, when represented in terms of variables that are scaled in such a manner. It was proven by statistical thermodynamics that the theorem of corresponding states rigorously applies if the intermolecular potential is of the form $u_0\varphi(\sigma/r)$, where u_0 and σ are parameters of the energy and of the separation [82]. The Lennard-Jones potential $u_{\mathrm{LJ}} = u_0((\sigma/r)^{12} - (\sigma/r)^6)$ is an example of such a potential. A reduced temperature $T^* = kT/u_0$ and a reduced density $\rho^* = \rho\sigma^3$ may be defined, allowing for a presentation of all thermodynamic properties in terms of the reduced variables. For a given function $\varphi(\sigma/r)$ the reduced critical data T_c^*, ρ_c^* and the phase diagrams in the reduced variables are independent of the particular values of u_0 and σ. Guggenheim's analysis of the phase diagrams of the liquid–gas phase transition of the noble gases [6] demonstrated not only the validity of the corresponding states approach for this group of compounds but showed also that the coexistence curves are in accordance with the Ising model but not with any mean-field theory.

Although the theorem of corresponding states can hardly apply rigorously in real systems, approximate validity is found quite often even in ionic solutions [69–71, 83, 84]. Otherwise, as emphasized by Guggenheim, the deviations from the corresponding state behaviour may give valuable hints on specific properties of the particular systems [6]. Thus, corresponding state analysis enables us to select certain groups in which the corresponding state principle is satisfied as was demonstrated, for example, by analysing surface tensions [85, 86] and phase diagrams [83, 84].

Considering ionic solutions, the RPM may be used as a reference system for the corresponding states analysis of the phase diagrams of ionic systems. Certainly, the RPM can only be a crude cartoon of a real ionic solution. The phase transition of this model is a liquid–gas transition. The RPM does not take into account the chemical structures of the ions of the ILs, the molecular correlations between the ions and the solvent molecules. Therefore, it is most remarkable that, besides the universal critical exponents, the critical properties of the RPM are in general agreement with those of the liquid–liquid phase transitions found in ionic solutions [69–71, 83, 84].

With an estimate of the smallest separation σ of the charge centres of the oppositely charged ions and the knowledge of the dielectric permittivity ε of the solvent the experimental data may be expressed in terms of the RPM variables, the reduced temperature T^* and the reduced density ρ^*:

$$T^* = \frac{kT\varepsilon\sigma}{q^2} \qquad \text{and} \qquad \rho^* = \rho\sigma^3, \tag{1}$$

where q is the charge of the ions and ρ the number density of all ions. Estimates of the critical data based on the critical data of the RPM have been a useful tool when searching

liquid–liquid phase transitions of ionic solutions [25, 58–60] at ambient conditions.

Until now, most work on phase transitions in ionic solutions concerns solutions in alcohols [12, 14–20, 25–27, 72–76]. Reports on liquid–liquid demixing in other solvents, e.g. in alkanes [70], arenes [23, 71, 77–79, 84, 87], alkylhalides [21, 80, 81] or other solvents as ethers [8–11, 24] are rare. The list of the work on liquid–liquid phase transitions is not exhaustive. For solutions in non-polar solvents the critical temperatures T_c^* in RPM variables have been found to be in the region but below the RPM value [70, 71] obtained in simulations [28–31]. For polar solvents, such as alcohols and water, it was observed that the reduced critical temperatures are larger than predicted by the RPM. An almost linear variation of T_c^* with the dielectric permittivity of the solvent [69, 83, 84] was observed, indicating a continuous change of the dominating forces driving the phase transitions from Coulomb interactions in non-polar solvents to a mechanism based on solvophobic interactions in solvents of high dielectric permittivity. It was also observed that phase diagrams of the solutions in protic solvents such as alcohols and water get a lower critical solution point when the analysis is carried out in terms of the RPM variables, taking into account the temperature dependence of the dielectric permittivity of the solvent. This observation is taken as an indication of the importance of the contribution of hydrophobic interactions to the phase transition [71, 84]. Conversely, the phase diagram of solutions in aprotic polar solvents that have a lower critical solution point such as, for example, solutions in SO_2 [88] or $HCCl_3$ [21] get an upper critical solution point in the phase diagrams represented in RPM variables so that the phase transition can be expected to be driven by Coulomb forces [21, 71] in spite of the lower critical solution point in the normal temperature scale.

In this work we continue our systematic study of the phase diagrams of ionic solutions aiming to identify general properties of the phase diagrams and searching for solutions appropriate for precise measurements of critical properties, crossover and asymmetry of the coexistence curves. We compare the experimental data with the simulation results for the primitive model, which we analyse in the same way as the experimental data. We report measurements of solutions of 1-n-octadecyl-3-methyl imidazolium ($C_{18}mim^+$) bistrifluormethylsulfonylimide (NTF_2) in tetralin, cyclohexane and methylcyclohexane, analyse the literature data of solutions of other $C_n mimNTF_2$ ILs in arenes and alcohols and compare with results of solutions of $C_n mimCl$ in arenes and CCl_4 as well as of $C_n mimBF_4$ in alcohols, which were discussed before [71, 84]. The analysis of the behaviour of solutions of ionic liquids with the NTF_2^- anion provides a particular challenge for the analysis because of the properties of the anion. While the Cl^- ion and the BF_4^- anion may reasonably well be approximated by a sphere so that the centre of charge is identical with the centre of mass, the NTF_2^- anion is by no means spherical. The NTF_2^- anion is flexible and allows for different conformers [89, 90]. The nitrogen atom in the anion is not necessary identical with the centre of mass and the centre of charges. The negative charges are expected to be distributed at the oxygen atoms. Consequently, for $C_n mimCl$ and $C_n mimBF_4$ reasonable estimates for the distance of the centres of charges at contact (taken as the effective hard-sphere diameter of the ions) were possible on the basis of van der Waals radii. Because this is not possible for the NTF_2^- anion we employ simulation results for the radial distribution function [91] for estimating the effective hard-sphere diameter and reanalyse the data concerning solutions of $C_n mimCl$ and $C_n mimBF_4$, using radial distribution functions given in the same work.

2. Methodology

2.1. Data analysis of phase diagrams

Presuming Ising criticality, the temperature dependence of a concentration variable X at coexistence near the critical temperature T_c can be represented by power series in terms of the reduced temperature $\tau = |T - T_c|/T_c$ [4, 5, 53], the so-called Wegner expansion:

$$\frac{X_\pm}{X_c} = \frac{X_m}{X_c} \pm B\tau^\beta(1 + B_1\tau^\Delta + B_2\tau^{2\Delta} + \cdots), \qquad (2)$$

where

$$\frac{X_m}{X_c} = 1 + A\tau + C\tau^{2\beta} + D\tau^{1-\alpha}(1 + D_1\tau^\Delta + \cdots). \qquad (3)$$

By X we denote a composition variable. The plus refers to the region $X > X_m$ and vice versa; X_m is the so-called diameter, defined by the average $X_m = (X_+ + X_-)/2$ of the compositions X_+ and X_- of the coexisting phases. For the Ising model the exponents assume the universal values $\beta = 0.325$, $\alpha = 0.11$ and $\Delta = 0.51$, where β is the leading exponent for the phase diagram, α is the exponent of the heat capacity and Δ is the crossover exponent, describing the crossover from Ising to classical mean-field behaviour. In mean-field theories $\beta = 1/2$ and $\alpha = 0$, so that the rectilinear diameter rule of Cailletet–Mathias, which assumes a linear temperature dependence of the diameter, applies in mean-field theory. By definition, there is no crossover exponent Δ in mean-field models. While the exponents are universal, the amplitudes are specific for the system but must satisfy certain sum rules. The corrections to scaling that are given in equations (2) and (3) suffice in the region $\tau < 10^{-2}$ [4]. When analysing data in a wider temperature region a crossover theory [45] should be applied. However, at large distances from the critical point other specific contributions become important so that universality is lost.

The non-analytic temperature dependence of the diameter was not noticed for a long time. Now the nonlinearity of the diameter is accepted although its temperature dependence is still under discussion [53–57]. For some time it was agreed that the term with the exponent $1 - \alpha$ is the leading term near the critical point, while the 2β term was regarded as the consequence of a non-appropriate choice of the concentration variable [92]. Recent theoretical work, termed complete scaling, that assumes three scaling fields suggests the 2β term as the leading part [54–57]. Another theory that assumes only two scaling fields but assumes a nonlinear relation between

the scaling fields and the physical fields [93] leads to the same conclusion. The 2β term becomes small for liquid–liquid phase transitions far apart from a liquid–gas critical point if the number density is chosen as the variable [45]. In many cases partial cancellation of the 2β and the $1-\alpha$ terms may cause an apparent linear temperature dependence of the diameter [55]. That's why deviations from linearity are often small. Therefore, it is difficult to determine uniquely the various coefficients of equation (3) by numerical analysis of experimental data. With the exception of [94] simulations of the RPM have not reached the accuracy to show the non-analytical contributions to the diameter of the phase diagram.

The analysis of phase diagrams using equations (2) and (3) or the crossover theories requires precise knowledge of the data of the critical point and measurements with mK accuracy. Most phase diagrams reported in the literature are obtained by the so-called visual method, where the temperature of the cloud point for samples of different compositions is measured. This method, which is also used in this work, is mostly not accurate enough to allow for a data analysis by equations (2) and (3) but suffices to estimate the locus of the critical point and show the gross features of the shape of the phase diagrams. Therefore, a simpler approach for the data evaluation may suffice here.

In engineering thermodynamics analytical Taylor expansions are commonly used for describing excess functions and coexistence curves. Using analytical functions, however, implies mean-field exponents for the critical properties, ignoring the fundamental fact that liquid–liquid phase transitions belong to the Ising universality class. Therefore, we apply a method [83], which is simpler than equations (2) and (3) but takes care of the non-classical nature of the phase diagrams. The simplified scaling laws applied in the analysis are

$$X_\pm - X_m = \pm b(T_\mathrm{c} - T)^{1/3} \tag{4}$$

where

$$X_m = X_\mathrm{c} + a(T_\mathrm{c} - T). \tag{5}$$

By using the small letters a and b in equations (4) and (5) we indicate that we use unscaled variables. Equations (4) and (5) lead to a cubic equation for T, which can be solved exactly. However, the resulting solutions are too messy to be applied in a fitting procedure. In many cases the slope of the diameter is not very large and an expansion of $|X - X_m|^3$ in first order of a may suffice. The resulting function $T(X)$, which will be used as a fitting function, is

$$T = T_\mathrm{c} - \frac{|X - X_\mathrm{c}|^3}{b^3 \pm 3a(X - X_\mathrm{c})^2}. \tag{6}$$

The positive and negative signs correspond to the range $X < X_\mathrm{c}$ and $X > X_\mathrm{c}$, respectively. For a lower critical solution point the sign in front of the fraction becomes positive. Alternatively, the signs of b and a may be changed for describing phase diagrams with a lower solution point. The parameters of the fit are the critical data T_c and X_c, the width b of the coexistence curve and the slope a of the diameter. By such a fit the non-classical shape of the phase diagrams is taken into account in a reasonable approximation. The approximation $\beta = 1/3$, which was also used by Guggenheim, is near the Ising value $\beta = 0.325$ and suffices for our purpose. Note, straightforward fits by an analytic power series not only imply classical exponents, but often also lead to erroneous descriptions, e.g. by showing spurious maxima.

As an alternative to the assumption of the validity of the rectilinear diameter rule we may assume that only one of the terms in equation (3) suffices. As the limiting case we take only the 2β term so that equation (5) is replaced by

$$X_m = X_\mathrm{c} + c(T_\mathrm{c} - T)^{2/3}. \tag{7}$$

Instead of equation (6) we get

$$T = T_\mathrm{c} - \frac{|X - X_\mathrm{c}|^3}{b^3 \pm 3cb|X - X_\mathrm{c}|}. \tag{8}$$

Equations (6) or (8) may also be applied for fitting corresponding states diagrams in terms of the reduced variables $\Delta X = (X - X_\mathrm{c})/X_\mathrm{c}$ and $\tau = |T - T_\mathrm{c}|/T_\mathrm{c}$. The fitted parameters are then termed A and B, or C and B because they correspond to the coefficients in equations (2) and (3):

$$\tau = \frac{|\Delta X|^3}{B^3 \pm 3A\Delta X^2} \tag{9}$$

$$\tau = \frac{|\Delta X|^3}{B^3 \pm 3BC|\Delta X|}. \tag{10}$$

In mean-field theory, the equations corresponding to equations (4) and (5) lead to a quadratic equation with a simple exact solution. The equations analogous to equations (6) and (9) become

$$T = T_\mathrm{c} - \frac{(X - X_\mathrm{c})^2}{b^2 + 2a(X - X_\mathrm{c})} \tag{11}$$

$$\tau = \frac{\Delta X^2}{B^2 + 2A\Delta X}. \tag{12}$$

From a rigorous theoretical point of view the physical variables temperature and composition must be replaced by some linear combination in order to achieve a transformation to the variables of the Ising model [54–57]. This is outside the scope of this work. From the experimental point of view various choices for the composition variable X can be thought of, e.g. the mole fraction x, the mass fraction w, the volume fraction φ or the number densities ρ_i of the components. Although much used in the technical literature, the mass fraction is not appropriate, because the masses are irrelevant for the thermodynamics of fluids. We report the data in terms of the mole fraction. We also analyse the data in terms of the reduced ion number density of the salt, the variable used in theories and simulations of the RPM. The application of the number density as variable, however, requires a knowledge of the density as a function of temperature and concentration. In a reasonable approximation, the densities can be estimated by assuming additive molar volumes, thus ignoring the excess volumes. In this approximation the reduced ion number density ρ^*, which is the corresponding state variable of the RPM, is estimated from the mole fraction x_IL of the IL and the molar volumes V_IL and V_S of the IL and of the solvent, respectively:

$$\rho^* = \frac{2x_\mathrm{IL}\sigma^3 N_\mathrm{A}}{x_\mathrm{IL}V_\mathrm{IL} + (1 - x_\mathrm{IL})V_\mathrm{S}}. \tag{13}$$

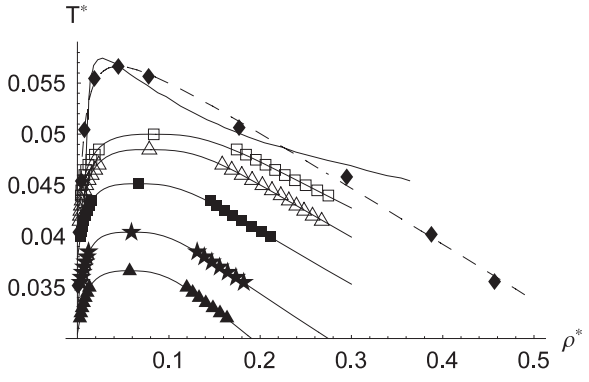

Figure 1. Phase diagrams of the primitive model [32] with equal charged hard spheres for axis ratios $\sigma^+/\sigma^- = \{1(\square), 2(\triangle), 3(\blacksquare), 4.26(\bigstar), 5.67(\blacktriangle)\}$ fitted with equation (6). The figure also shows the data (♦) of the early simulation [37] of the RPM that did not use a finite size scaling technique fitted with equation (11), presuming a mean-field criticality (dashed line) together with the phase diagram predicted by the Fisher–Levine theory.

Table 1. Parameters of the phase diagrams of charged hard spheres and the Lennard-Jones fluid. The critical temperatures T_c^* and the critical densities ρ_c^* are given in the reduced variables of the models. The coefficients of the width b and the slope a of the diameter are related to those scales, while the coefficients B and A refer to the corresponding state representation.

System	λ	T_c^*	ρ_c^*	b	a	B	A	Reference
LJ		1.2327	0.3366	0.518	0.22	1.65	0.79	[30]
RPM92[a]	1	0.0566	0.0447	0.940	8.97	5.01	11.36	[37]
RPMFL[a]	1	0.0572	0.0273	0.540	7.77	4.73	16.30	[2]
RPM	1	0.0500	0.0836	0.628	8.23	2.77	4.92	[31]
PM	2	0.0485	0.0787	0.581	7.29	2.69	4.49	[31]
PM	3	0.0452	0.0666	0.512	7.10	2.74	4.81	[31]
PM	4.26	0.0404	0.0591	0.453	6.24	2.63	4.27	[31]
PM	5.57	0.0366	0.0571	0.433	5.22	2.52	3.35	[31]
RPM	1	0.0499	0.0809	0.609	7.59	2.77	4.69	[32]
PM	1.33	0.0500	0.0840	0.636	7.03	2.79	4.19	[32]
PM	2	0.0490	0.0700	0.510	7.00	2.60	5.00	[32]
PM	4	0.0436	0.0512	0.391	5.48	2.69	4.66	[32]

[a] Fits use equations (9) and (10), which presume mean-field behaviour.

N_A is Avogadro's number. The diameter σ of the ions is identical with the charge separation in the hard-sphere models RPM and PM. In the analysis of the experimental phase diagrams we take here the maximum of the pair correlation function for the mass centre of the imidazolium ring of the cation and the centre of mass of the anion [91] as an estimate of σ. With this choice we adapt the RPM variables, given in equations (1) and (13), for the analysis of real ionic solutions. The volume fraction φ would be obtained by replacing $2\sigma^3 N_A$ in the nominator of equation (13) by the molar volume V_{IL} of the salt.

2.2. *Phase diagrams of model systems*

A complete theory which treats the non-classical singularities at the critical point of ionic fluids adequately and which predicts the coefficients in equations (2) and (3) correctly is not available. This is true even for the simplest model of an ionic fluid, the RPM. Thus we can only compare experimental results with simulation results of the model of equal-sized charged hard spheres, the RPM, and of its generalization, the PM, concerning ions of differing sizes. In figure 1 we see the phase diagrams reported for the primitive model [32] with equal charged hard spheres for axis ratios $\lambda = \sigma + /\sigma - = \{1(\square), 2(\triangle), 3(\blacksquare), 4.26(\bigstar), 5.67(\blacktriangle)\}$. The temperature scale and the density scale are that of the RPM defined in equation (1), where the diameter σ is the mean value of the diameters σ^+ and σ^- of the anion and the cation, respectively. The curves are the results of the fits using equation (6). The results of the numerical analysis of the phase diagrams are given in table 1. The relative uncertainties of the parameters of the fit are $\Delta T_c^* = 0.15\%$, $\Delta\rho_c^* = 0.8\%$, $\Delta b = 0.6\%$ and $\Delta a = 2.7\%$.

From figure 1 it can be seen that both the critical temperature and the critical density are shifted towards smaller values with increasing asymmetry of the ion size. The figure shows also the simulation results (♦) of the early simulation [37] of the RPM that did not use a finite size scaling technique fitted with equation (11) presuming mean-field criticality (dashed line) together with the phase diagram predicted by the FL theory. The phase diagram obtained from the FL theory was also fitted using equation (11) but restricted to the density range below 0.1. The early simulation, which we may term mean-field simulation, yields a critical point that is at a 10% higher temperature and at a density that is smaller by almost 50% if compared to the simulation using finite size scaling. The FL theory yields a slightly higher critical temperature and a density which is smaller by almost a factor of two.

The trends of the locus of the critical points are displayed in figures 2 showing the critical temperatures (a) and the critical densities (b) obtained from the analysis of the simulation data of [32] (♦) and [33] (□) as a function of the size ratio σ^+/σ^- of the ions. It appears that the critical temperature is changed little if the axis ratio is between one and two and decreases almost linearly for larger axis ratios. The critical temperature obtained from the mean-field simulation (★) [37] is not to distinguish from that of the FL theory [2] in this scale. The critical densities decrease with the axis ratio in a bell-shaped manner. However, this variation is small if compared to the difference between the density obtained by simulations of the RPM ($\sigma^+/\sigma^- = 1$) that apply the FSS techniques and that obtained from the mean-field simulation (★) and the FL theory (■).

It is difficult to judge the change of the parameters describing the shape of the phase diagrams from the diagrams in figure 1. Therefore we show in figures 3(a) and (b) the parameters of the width b^* and of the slope a^* of the diameter of the phase diagrams as a function of the relative size of the ions, obtained from the fits using equation (6). By the star we indicate that the reduced variables of the RPM are used. Both the width and the slope of the diameter of the phase diagrams decrease with the asymmetry of the phase diagrams. Again we have included the results of the fits to the mean-field simulation of the RPM (★) and the FL theory (■). From the data of

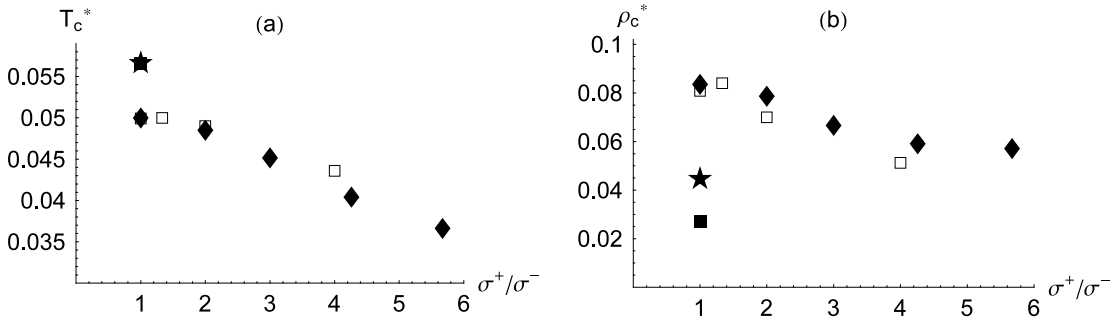

Figure 2. Critical temperatures (a) and critical densities (b) of the primitive model obtained from the analysis of the simulation data of [32] (♦) and [33] (□) as a function of the size ratio $\lambda = \sigma^+/\sigma^-$ of the ions. The point labelled (★) refers to the early simulation that did not use finite size scaling, while the point labelled (■) gives the result of the Fisher–Levin theory.

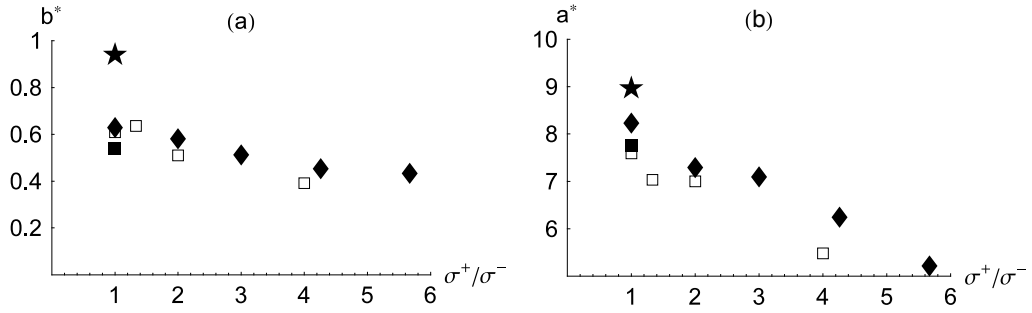

Figure 3. Parameters of (a) the width b^* and (b) the slope a^* of the primitive model of the diameter of the phase diagrams as a function of the relative size of the ions. The symbols have the same meaning as in figure 2.

the mean-field simulation we get values larger than that of the simulations using finite size scaling techniques. Fortuitously the parameters obtained by fitting the phase diagram predicted by the FL theory agree remarkable well with those obtained from the simulations using finite size scaling.

As outlined in section 1, corresponding state behaviour can be expected if the intermolecular potential is of the same form, which is not the case for different axis ratios considered in the primitive model. Nevertheless, it is of interest to see if the trends of the shape parameters remain, when using the corresponding state variables $\Delta\rho^* = |\rho^* - \rho_c^*|/\rho_c^*$ and $\tau^* = |T^* - T_c^*|/T_c^*$. Note that the corresponding state representation is independent of the figures of σ and ε because these parameters are constant and cancel in the corresponding state variables. In figure 4 we compare the corresponding state phase diagrams of the RPM, of the PM with that of the Lennard-Jones fluid (♦) [33] and that of the rare gases (◊) taken from Guggenheim's paper [6]. We include the fits to the mean-field simulation (dashed line) of the RPM and the FL theory (full line).

The symbols have the same meaning as in figure 1. The phase diagrams of the Lennard-Jones fluid and of the noble gases are very similar: they are quite symmetric and much narrower if compared to the ionic fluids. The curve is the fit to the simulation results of the Lennard-Jones fluid. The phase diagram of the RPM has the most asymmetric shape among the ionic fluids considered in the simulations. The drawn curve is the fit to the RPM. Note that the simulations

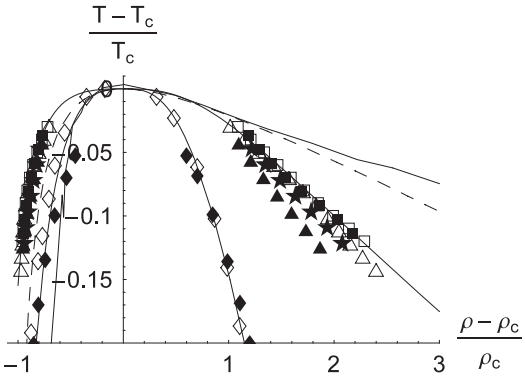

Figure 4. Corresponding state phase diagrams of the PM. The symbols denote the same systems as in figure 1. The shown fit concerns the RPM. The figure includes the data of the rare gases (◊) [6] and the simulation data of the Lennard-Jones fluid (♦) [33] with the fit and also the fits to the early simulation of the RPM (dashed line) and the FL theory (full line) which yield more asymmetric phase diagrams.

approach the critical temperature only until $\tau \cong 0.03$ which corresponds to a temperature separation of about 10 K from the critical temperature in the investigations of ionic solutions at ambient temperatures. The asymmetry obtained in the mean-field simulation of the RPM is larger than that of FSS simulations. The FL theory yields an even larger asymmetry.

These observations are more clearly demonstrated in figures 5(a) and (b) showing the width and the diameter slope

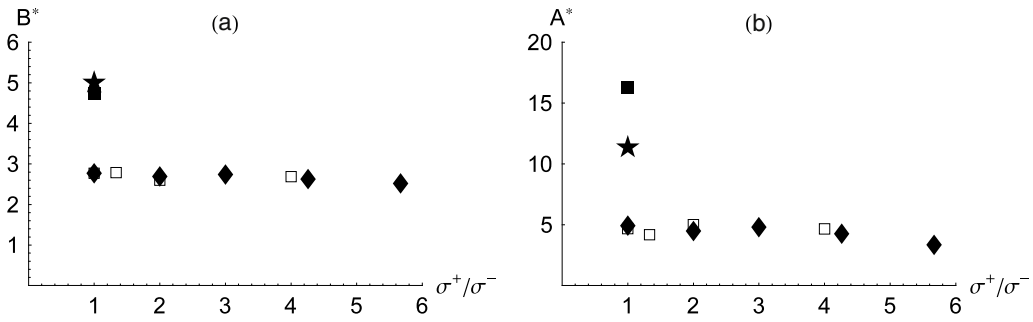

Figure 5. Parameters of (a) the width B^* and (b) the slope A^* of the diameter of the corresponding state phase diagrams as a function of the relative size of the ions. The symbols refer to the same systems as in figure 2.

of the corresponding state phase diagrams, respectively. The width of corresponding state phase diagrams of the PM is almost independent from the axis ratio of the ions. The decrease with the size of the axis ratio is almost not noticeable if compared to the larger width obtained from the mean-field simulation and the FL theory. A similar conclusion applies to the asymmetry parameter A^*. Thus, the trends of the parameters of the corresponding state phase diagrams of the primitive model are the same as that in the RPM variables shown in figure 3. However, the relative changes are much smaller, due to the scaling by the critical data. Remarkably the difference between the parameters obtained from the classical simulations and the FL theory for the RPM to the FSS simulations is enhanced when corresponding state variables are used.

So far we have discussed the results of the fits to the phase diagram yielded by the analytical FL theory. The advantage of analytical theories, however, to provide a complete solution for the thermodynamic space, is not exploited. Close to the critical point the explicit expressions for the free energy density can be written as a power series in terms of the corresponding state variables. The coefficients in this expansion, known as the Landau expansion, although already given by van der Waals, can be calculated from the theory. The Landau expansion allows calculating asymptotic expressions for the width B^* and the slope A^* of the diameter of the coexistence curve [71, 95]. The exact asymptotic results for the quantities B^* and A^* in the FL theory are 3.87 and 11.6, which is somewhat below the figures obtained by fitting the data of the phase diagram in the temperature range $\tau^* < 0.1$ which includes already some non-asymptotic contributions.

2.3. Experimental details

The ionic liquid 1-methyl-3-octadecylimidazolium-bis (trifluormethylsulfonyl)-imid (C_{18}mimNTF$_2$) was purchased from Iolitec (Denzlingen, Germany). The purity certified by the producer was >98%. The solvents were chosen of highest quality available cyclohexane (Fluka >99.5%), methylcyclohexane (Sigma-Aldrich >99%) and cis-tetralin (Fluka >98.%). Standard NMR and MS analysis did not show impurities in the salt and the solvents. The salt was filled into the sample cell inside a glove box filled with argon and dried by keeping it at 80 °C for 24 h under the oil pump vacuum of 5×10^{-5} bar. The solvents were dried by adding P_2O_5. The 'pump and freeze' technique at the vacuum line was used to remove the gases and volatile compounds from the solvents and from the salt. The dried solvents were condensed via a vacuum line into the sample cell that was cooled with liquid nitrogen. A Teflon tap (Normag) attached to the sample cell enabled connecting and removing the sample cell from the vacuum line, thus allowing control of the weight of the sample during the drying process, and also when changing the solvent content. The concentrations were determined by weight with an accuracy of 10^{-4} g. In this manner a set of concentrations was prepared by adding or removing solvent from the sample by distillation on the vacuum line with identical sample of the IL. Using this method the amount of the ionic liquid is constant; uncontrollable traces of impurities are avoided that can cause deformations of the separation curves, when different samples are investigated. Mixtures with the mass fractions ranging from 0.05 to 0.15 were prepared in this way. The cloud points were determined visually by repeated cooling of the homogeneous mixture in a thermostat with glass windows (Lauda K20KP) filled with water so that the accessible temperature range was 16–90 °C. Clearly, the accuracy of the visual method is limited by the subjectivity of the experimentalist. The cloud points have been measured in a temperature region of 1 K below the critical point for 10–16 different concentrations. The temperature was controlled with an accuracy of 0.01 °C using a Quartz thermometer (Hereaus QUAT200).

3. Results and discussion

3.1. Phase diagrams of solutions C_{18}mimNTF$_2$ in non-polar solvents

In figure 6 we show the phase diagrams for the solutions of 1-methyl-3-octadecylimidazolium-bis(trifluormethylsulfonyl)-imid (C_{18}mimNTF$_2$) in decalin (cis-decahydronaphtalene), cyclohexane and methylcyclohexane (figures 6(a)–(c)) as a function of the mole fraction x of the salt. The data of the phase diagrams are given in table 2. The last row of the table gives the data of the critical point determined by the equal volume criterion, which defines the critical concentration as that yielding equal volume for the phases just below the critical temperature. The measurements were carried out strictly preventing contact

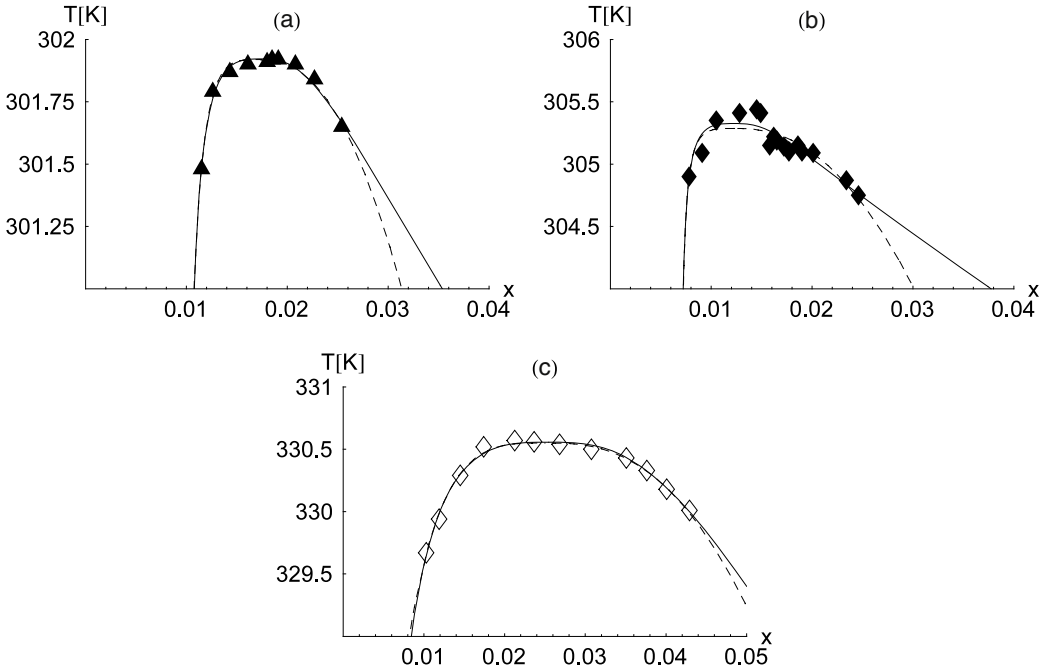

Figure 6. Phase diagrams of C_{18}mimNTF$_2$ (1-methyl-3-octadecylimidazolium-bis(trifluormethylsulfonyl)imid) in (a) methylcyclohexane, (b) cyclohexane and (c) decalin with the mole fraction as variable of the composition.

Table 2. Phase diagrams of solutions of C_{18}mimNTF$_2$ in the cyclic hydrocarbons cyclohexane, methylcyclohexane and decalin. The last row gives the critical data as determined by the equal volume criterion.

C_6H_{12}		C_7H_{14}		$C_{10}H_{18}$	
x	T (K)	x	T (K)	x	T (K)
0.0246	304.75	0.0115	301.48	0.0102	329.66
0.0234	304.87	0.0126	301.79	0.0118	329.94
0.0201	305.09	0.0143	301.87	0.0144	330.28
0.0190	305.10	0.0161	301.90	0.0174	330.52
0.0186	305.15	0.0180	301.91	0.0212	330.57
0.0177	305.10	0.0185	301.92	0.0236	330.55
0.0172	305.14	0.0191	301.92	0.0268	330.53
0.0165	305.19	0.0208	301.90	0.0307	330.50
0.0162	305.22	0.0227	301.84	0.0350	330.42
0.0158	305.15	0.0254	301.65	0.0376	330.33
0.0149	305.41			0.0400	330.17
0.0145	305.44			0.0429	330.01
0.0128	305.41				
0.0105	305.35				
0.0091	305.09				
0.0078	304.90				
x_c	T_c (K)	x_c	T_c (K)	x_c	T_c (K)
0.0162	305.22	0.0185	301.92	0.0236	330.55

of the solutions with air. Using the vacuum line for the sample preparation and drying the solvents with P_2O_5 is essential. Without such precautions reasonable phase diagrams cannot be obtained in non-polar solvents because the separation temperatures are very sensitive to traces of humidity.

The data of the systems cover only the small temperature range of about 1 K. We have fitted the data assuming the validity of the rectilinear diameter rule by equation (6) (full line) or by equation (8) (dashed line), describing the diameter by the 2β term. The parameters obtained from the fits are contained in table 3, which lists the critical temperatures T_c and the critical mole fraction x_c together with the coefficient b_x determining the width and the coefficients a_x and c_x that describe the asymmetry of the phase diagrams in equations (6) and (8), respectively. The table gives the parameters for the systems reported here and others taken from the literature that will be discussed later on in this paper. The table also gives the parameters of the corresponding state diagrams $B_x A_x$ and C_x. The parameters in the rows in which the systems are labelled by a star are obtained by fitting equation (8) to the data. Those rows give the parameter $c_x[\mathrm{K}^{-2/3}]$ and C_x instead of $a_x[\mathrm{K}^{-1}]$ and A_x as in all other rows. The root mean square deviations of the parameters as given by the fits are better than $\Delta T_c = 0.04$ K, $\Delta x_c = 5.4\%$, $\Delta b_x = 10\%$ and $\Delta a_x = 20\%$, $\Delta c_x = 20\%$.

All systems have an upper critical solution point (UCSP), where the critical temperatures decrease in the order: decalin, cyclohexane, methylcyclohexane. The critical mole fractions are all located at small mole fractions below 0.03. The critical concentrations estimated from the fits do not differ systematically from the values obtained experimentally by applying the equal volume criterion, given in table 2. In an ideal experiment the maximum of the experimental data, the critical point determined by the equal volume criterion and the critical data determined by the fit should be the same, which is not achieved in the experiment in spite of many efforts. The figures obtained for T_c, x_c and b_x are almost invariant against the choice of the function describing the diameter. In the corresponding state diagrams the diameter slopes come out unreasonably large when fitting equation (9) to the data. Therefore figure 7 shows only the fits with equation (10).

Other choices of the concentration variable rather than x are useful for further analysis. We analyse the data with the RPM density ρ^* as variables for the composition. For transforming the mol fractions into the RPM densities

Table 3. Parameters of the phase diagrams of solutions of ionic liquids with the NTF_2^- anion with the mole fraction as a variable of the composition.

System	T_c (K)	x_c	b_x ($K^{-1/3}$)	a_x (K^{-1})	B_x	A_x	ε_c	Reference
C_{18}mimNTF_2/m-c-hexane	301.92	0.017	0.0100	0.0055	3.88	96.41	2.01	
C_{18}mimNTF_2/c-hexane	305.33	0.012	0.0082	0.0061	4.52	153.56	2.00	
C_{18}mimNTF_2/decalin	330.56	0.025	0.0185	0.0036	5.02	47.12	2.13	
C_{18}mimNTF_2/m-c-hexane[a]	301.99	0.017	0.0105	0.0048	4.18	12.69	2.01	
C_{18}mimNTF_2/c-hexane[a]	305.29	0.012	0.0101	0.0065	5.65	24.40	2.01	
C_{18}mimNTF_2/decalin[a]	330.55	0.025	0.0188	0.0040	5.26	7.71	2.18	
C_2mimNTF_2/C_3OH	294.06	0.137	0.0692	0.0054	3.36	11.55	20.87	[75]
C_2mimNTF_2/C_4OH	320.64	0.146	0.0751	0.0062	3.53	13.66	14.77	[75]
C_2mimNTF_2/C_5OH	339.84	0.162	0.0852	0.0076	3.67	15.95	10.57	[75]
C_4mimNTF_2/C_4OH	300.08	0.139	0.0724	0.0056	3.49	11.99	16.99	[74]
C_4mimNTF_2/C_6OH	333.01	0.202	0.0883	0.0041	3.03	6.78	9.37	[74]
C_3mmimNTF_2/C_4OH	334.18	0.155	0.0724	0.0042	3.23	8.99	13.36	[74]
C_3mmimNTF_2/C_6OH	374.28	0.247	0.0954	0.0023	2.78	3.55	6.87	[74]
C_6mimNTF_2/C_6OH	306.32	0.146	0.0777	0.0062	3.58	12.99	11.45	[101]
C_8mimNTF_2/benzene	373.21	0.029	0.0093	0.0002	2.31	2.09	2.12	[77]
C_{10}mimNTF_2/benzene	318.50	0.019	0.0078	0.0004	2.82	5.98	2.23	[77]
C_{10}mimNTF_2/toluene	339.99	0.025	0.0105	0.0008	3.00	11.70	2.26	[77]
C_8mimNTF_2/α-styrene	429.51	0.052	0.0156	0.0003	2.28	2.39	2.11	[77]
C_{10}mimNTF_2/α-styrene	342.82	0.034	0.0124	0.0005	2.56	4.82	2.22	[77]

[a] The fits are based on equations (8) and (10). The parameters given in the columns, labelled a_x and A_x, are the parameters c_x and C_x, respectively, where the dimension of c_x is ($K^{-2/3}$).

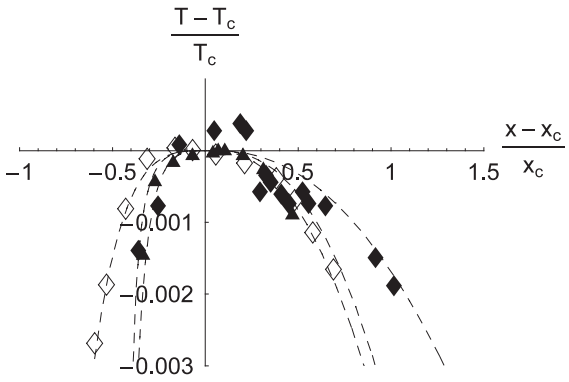

Figure 7. Corresponding state phase diagrams of solutions of C_{18}mimNTF_2 in (▲) methylcyclohexane, (♦) cyclohexane and (◊) decalin with the mole fraction x as a variable of the composition.

using equation (13) the densities of the salt [96] and of the solvents [97] are required and a value for the anion–cation separation σ. Equation (13) implies neglecting the excess volume, which can be obtained from density measurements of the solutions. Such measurements, however, are not available for the systems investigated and are outside the scope of this work. Excess volumes are expected to be positive [98] but too small to affect our considerations.

For the anion–cation separation σ we take the value of 5.4 Å, which is the maximum of the radial distribution function of the geometrical centres of the NTF_2 anion and of the imidazolium ring of the cation obtained in the simulations [91] of C_2mimNTF_2. X-ray analysis yielded 5.2 Å [90]. We take the value of the simulation [91] because it provides also the data for the C_2mimCl and C_2mimBF_4 that are needed later on. Table 4 contains the parameters T_c, ρ_c, b_ρ, $a_\rho(c_\rho)$, B_ρ and $A_\rho(C_\rho)$ of solutions of ionic liquids with the NTF_2^- anion obtained by fitting the data with the RPM density as a variable of the composition. The critical temperatures resulting from the fit are not changed by the choice of the variable; curves are somewhat more symmetrical. We pause to show the phase diagrams. The parameters of the fits are discussed later together with that of other systems.

In order to allow comparison of experimental data with the simulation results of the model fluids the temperatures are transformed into the RPM temperature scale, which requires dielectric permittivities of the solvents as a function of the temperature [99, 100]. Table 5 gives the parameters to the corresponding fits of the phase diagrams. For the three systems the critical temperatures are very similar as are the critical densities and the parameters of the width. Both the critical temperatures and the critical densities are smaller than the RPM values. The width parameters b and B are near the RPM values. The asymmetry parameters take values of the order of the RPM figures only with the fit by equations (8) and (10) describing the diameter by the 2β term.

To visualize the relations between the phase diagrams of the model systems and the studied solutions we show in figure 8 the corresponding state diagrams compared to that of the Lennard-Jones fluid (small dashed line) and the RPM (long dashed line). It is remarkable that the phase diagrams reported in this work are wider and more asymmetric than the phase diagram of the RPM, which certainly is wider and more asymmetric than the Lennard-Jones fluid.

3.2. Overview on the parameters of the phase diagrams

In order to get a comprehensive overview on the parameters characterizing the phase diagrams of the liquid–liquid phase transitions in ionic solutions we compare the data of the systems reported in this work with that of solutions of other ionic liquids in polar and non-polar solvents. The discussion is focused on solutions of ILs with imidazolium cations differing

Table 4. Parameters of the phase diagrams of solutions of ionic liquids with the NTF_2^- anion with the RPM density as a variable of the composition.

System	T_c (K)	ρ_c	b_ρ ($K^{-1/3}$)	a_ρ (K^{-1})	B_ρ	A_ρ	ε_c	Reference
C_{18}mimNTF_2/m-c-hexane	301.92	0.025	0.014	0.0071	3.67	85.42	2.01	
C_{18}mimNTF_2/c-hexane	305.33	0.020	0.013	0.0091	4.30	137.37	2.01	
C_{18}mimNTF_2/decalin	330.55	0.028	0.019	0.0032	4.78	37.86	2.18	
C_{18}mimNTF_2/m-c-hexane[a]	301.92	0.025	0.014	0.0062	3.92	11.32	2.01	
C_{18}mimNTF_2/c-hexane[a]	305.29	0.020	0.016	0.0093	5.26	21.23	2.01	
C_{18}mimNTF_2/decalin[a]	330.55	0.027	0.019	0.0035	4.93	6.18	2.18	
C_2mimNTF_2/C_3OH	294.13	0.248	0.097	0.0029	2.60	3.49	20.86	[75]
C_2mimNTF_2/C_4OH	320.58	0.219	0.096	0.0053	3.01	7.79	14.72	[75]
C_2mimNTF_2/C_5OH	339.84	0.215	0.096	0.0051	3.10	8.03	10.56	[75]
C_4mimNTF_2/C_4OH	300.12	0.210	0.087	0.0026	2.78	3.67	16.99	[74]
C_4mimNTF_2/C_6OH	333.05	0.222	0.080	0.0017	2.51	2.52	9.36	[74]
C_3mmimNTF_2/C_4OH	334.37	0.223	0.081	0.0018	2.52	2.72	13.34	[74]
C_3mmimNTF_2/C_6OH	374.15	0.260	0.083	0.0002	2.30	0.27	6.88	[74]
C_6mimNTF_2/C_6OH	306.37	0.171	0.075	0.0032	2.98	5.67	11.45	[101]
C_8mimNTF_2/benzene	373.12	0.051	0.016	0.0002	2.19	1.55	2.12	[77]
C_{10}mimNTF_2/benzene	318.49	0.036	0.014	0.0006	2.69	4.95	2.23	[77]
C_{10}mimNTF_2/toluene	339.98	0.038	0.016	0.0011	2.84	10.12	2.26	[77]
C_8mimNTF_2/α-styrene	429.34	0.059	0.017	0.0003	2.17	2.04	2.11	[77]
C_{10}mimNTF_2/α-styrene	342.81	0.044	0.015	0.0005	2.42	3.94	2.22	[77]

[a] The fits are based on equations (8) and (10). The parameters given in the columns, labelled a_ρ and A_ρ are the parameters c_ρ and C_ρ, respectively, where the dimension of c_ρ is ($K^{-2/3}$).

Table 5. Parameters of the phase diagrams of solutions of ionic liquids with the NTF_2^- anion represented by the RPM variables.

System	T_c^*	ρ_c^*	b^*_{RPM}	a^*_{RPM}	B^*_{RPM}	A^*_{RPM}	ε_c	Reference
C_{18}mimNTF_2/m-c-hexane	0.020	0.025	0.36	127.45	3.87	100.66	2.01	
C_{18}mimNTF_2/c-hexane	0.020	0.020	0.35	175.03	4.66	174.44	2.01	
C_{18}mimNTF_2/decalin	0.024	0.028	0.49	52.71	5.06	44.88	2.18	
C_{18}mimNTF_2/m-c-hexane[a]	0.020	0.025	0.38	4.23	4.14	12.63	2.01	
C_{18}mimNTF_2/c-hexane[a]	0.020	0.020	0.42	6.72	5.70	24.89	2.01	
C_{18}mimNTF_2/decalin[a]	0.024	0.027	0.49	2.28	5.22	6.92	2.18	
C_2mimNTF_2/C_3OH	0.200	0.248	−1.14	−4.77	−2.69	−3.86	20.86	[75]
C_2mimNTF_2/C_4OH	0.154	0.219	−1.14	−8.76	−2.78	−6.16	14.72	[75]
C_2mimNTF_2/C_5OH	0.117	0.215	−1.19	−9.97	−2.72	−5.44	10.56	[75]
C_4mimNTF_2/C_4OH	0.167	0.210	−1.03	−4.25	−2.70	−3.37	16.99	[74]
C_4mimNTF_2/C_6OH	0.102	0.222	−1.03	−3.58	−2.17	−1.64	9.36	[74]
C_3mmimNTF_2/C_4OH	0.146	0.223	−0.96	−2.98	−2.26	−1.95	13.34	[74]
C_3mmimNTF_2/C_6OH	0.084	0.262	−1.10	−0.20	−1.84	−0.07	6.88	[74]
C_6mimNTF_2/C_6OH	0.115	0.171	−0.95	−6.36	−2.71	−4.27	11.45	[101]
C_8mimNTF_2/benzene	0.026	0.051	0.43	4.64	2.51	2.37	2.12	[77]
C_{10}mimNTF_2/benzene	0.024	0.036	0.38	10.63	2.99	6.80	2.23	[77]
C_{10}mimNTF_2/toluene	0.025	0.038	0.43	24.81	3.31	16.23	2.26	[77]
C_8mimNTF_2/α-styrene	0.030	0.059	0.46	5.43	2.40	2.71	2.11	[77]
C_{10}mimNTF_2/α-styrene	0.025	0.044	0.39	8.36	2.58	4.76	2.22	[77]

[a] The fits are based on equations (8) and (10). The parameters given in the columns, labelled a^*_ρ and A^*_ρ, are the parameters c^*_ρ and C^*_ρ respectively, which are dimensionless as are all parameters in this table.

in the length of the side chains and the NTF_2^- anion. Solutions of imidazolium ILs with the anions Cl^- [70, 71, 84] and BF_4^- [69, 83] which were discussed before are included into the discussion. Parameters of the phase diagrams of ILs with the NTF_2^- anion are listed in tables 3, 4 and 5 for the different sets of variables. Tables with the parameters of the phase diagrams involving ILs with the anions BF_4^- and Cl^- are given in the appendix.

Figures 9(a) and (b) show some examples of the phase diagrams in non-polar and polar solvents. In figure 9(a), we see the phase diagrams of the solutions of C_{18}mimNTF_2 in methylcyclohexane, cyclohexane and decalin (◊), of solutions of C_{10}mimNTF_2 and C_8mimNTF_2 in benzene, and α-styrene (△) [101]; figure 9(b) concerns solutions of C_2mimNTF_2 in propanol, butanol and pentanol (□) [75] and of C_3mmimNTF_2 in hexanol (☆) [74]. In the C_3mmim anion the acidic proton at the carbon atom between the nitrogen atoms of the imidazolium ring is substituted by a methyl group, so that C_3mmimNTF_2 may be expected to be a less polar isomer of C_4mimNTF_2. As generally in this paper the systems are listed in the order of increasing critical temperatures. The curves connecting the points of the C_{18}mimNTF_2 solutions are fits using equation (8), while all other curves are described by equation (6). The critical concentrations of the solutions in alcohols are near the mole fraction of 0.1, while the critical

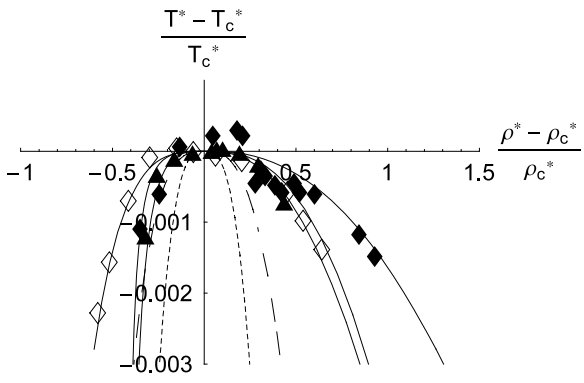

Figure 8. Corresponding state phase diagrams of solutions of C_{18}mimNTF$_2$ in (▲) methylcyclohexane, (♦) cyclohexane and (◊) decalin based on the RPM variables compared to that of the RPM (long dashed) and the Lennard-Jones fluid (short dashed).

mole fractions are below 0.04. As is well known, the critical temperatures of the alcohol solutions decrease with increasing polarity of the solvent [69–75], which is in accordance with the expectation that the stability of the ionic solution increases with the polarity of the solvent. A qualitative rationalization for the critical temperatures of the non-polar solutions is not so straightforward.

3.2.1. Critical temperatures. We include solutions of ILs with the anions BF_4^- [69, 74, 83] and Cl^- [71, 84] in the discussion of the parameters of the phase diagrams, which are given in the tables of the appendix. Figure 10(a) shows the dependence of the critical temperature T_c on the dielectric permittivity $\varepsilon_c(T_c)$ of the solvent at the critical temperature for the solutions $C_n$mimNTF$_2$ salts in non-polar solvents and alcohols. The figures of the dielectric permittivities of the solvents are taken from [99, 100].

The data are labelled as follows: (◊) C_{18}mimNTF$_2$ in methylcyclohexane, cyclohexane and decalin, (▲) C_{10}mimNTF$_2$ in benzene, toluene and α-styrene, C_8mimNTF$_2$ in benzene and α-styrene [77], (□) C_2mimNTF$_2$ in propanol, butanol and pentanol [75], (△) C_4mimNTF$_2$ in butanol and hexanol [74], (☆) C_3mmimNTF$_2$ in butanol and hexanol [74] and (★) C_6mimNTF$_2$ in hexanol [101]. The systems described by the same symbol are listed in the order of increasing separation temperatures.

In figure 10(a) we can identify two different groups of data. For the solutions in the alkanes and arenes the critical temperatures are not correlated with the dielectric permittivity. The solutions of salts with the anions with longer side chains are more stable, resulting in a lower critical temperature. For the solutions in alcohols the critical temperatures decrease with the dielectric permittivity, which is qualitatively in accordance

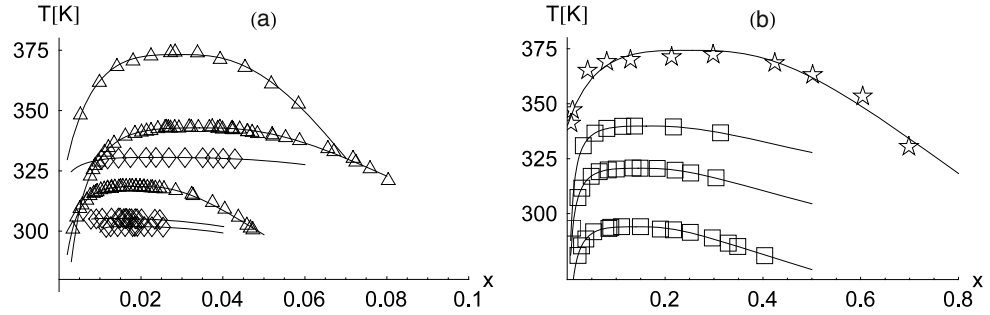

Figure 9. Phase diagrams of the solutions of ILs in (a) non-polar aprotic solvents (C_{18}mimNTF$_2$ in methylcyclohexane, cyclohexane and decalin (◊), of solutions of C_{10}mimNTF$_2$ and C_8mimNTF$_2$ in benzene, and of C_{10}mimNTF$_2$ in α-styrene (△) [77]) and (b) alcohols (C_2mimNTF$_2$ in propanol, butanol and pentanol (□) [75] and of C_3mmimNTF$_2$ in hexanol (☆) [74]). The systems are listed in the order of increasing critical temperatures.

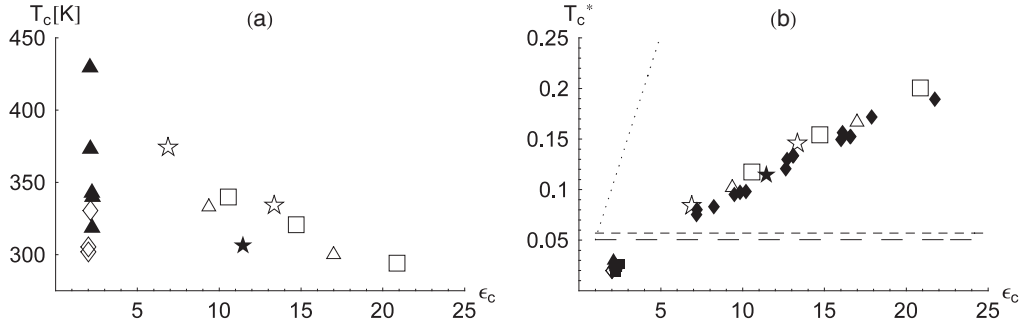

Figure 10. Variation of the critical temperature of ionic solutions with the dielectric permittivity of the solvents at the critical temperatures. (a) Critical temperatures as observed in the Kelvin scale; (b) critical temperatures in the RPM temperature scale. The long dashed line is the simulation result of the RPM. The short dashed line is the result of FL theory, while the dotted line is 0.05ε. The data are labelled as follows: (◊) C_{18}mimNTF$_2$ in methylcyclohexane, cyclohexane and decalin, (▲) C_{10}mimNTF$_2$ in benzene, toluene and α-styrene, C_8mimNTF$_2$ in benzene and α-styrene [77], (□) C_2mimNTF$_2$ in propanol, butanol and pentanol [75], (△) C_4mimNTF$_2$ in butanol and hexanol [74], (☆) C_3mmimNTF$_2$ in butanol and hexanol [74], (★) C_6mimNTF$_2$ in hexanol [101], (♦) (C_6mimBF$_4$, C_4mimBF$_4$) in alcohols (n-propanol, n-butanol, n-pentanol, n-hexanol, n-octanol, 2-pentanol, 2-butanol, i-butanol, t-butanol) [69, 74] and (■) C_{12}mimCl in benzene, toluene, o-xylene, and tetralin and C_{14}mimCl in CCl_4 [71].

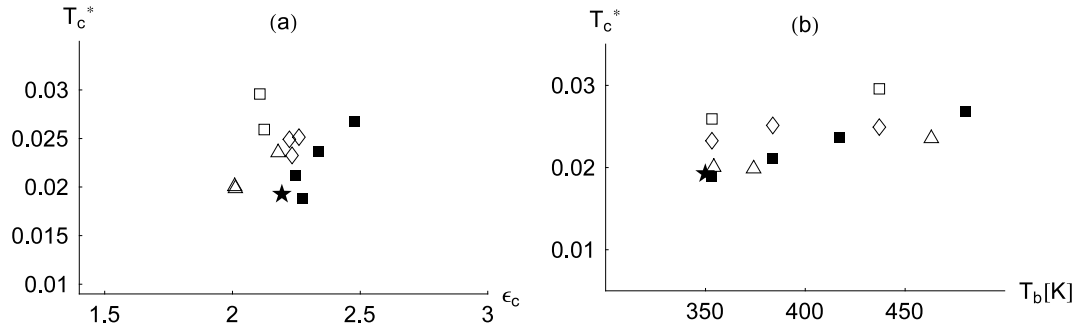

Figure 11. RPM critical temperatures T_c^* of ionic solutions in non-polar solvents as a function of (a) the dielectric permittivity and (b) the boiling temperatures of the solvents. The systems are labelled as follows: (□) C_8mimNTF2 in benzene and α-styrene, (◊) C_{10}mimNTF2 in benzene, toluene and α-styrene [77], (△) C_{18}mimNTF$_2$ in methylcyclohexane, cyclohexane and decalin, C_{12}mimCl in (■) benzene, toluene, o-xylene and tetralin and (★) CCl_4.

with the expectation based on the RPM: the stability of ionic solutions is expected to increase with the dielectric permittivity of the solvent, thus lowering the critical temperature. Although the IL C_3mmimNTF$_2$ is expected to be less polar than the isomeric C_4mimNTF$_2$ and hence better soluble in alcohols, it turns out that the solutions of C_3mmimNTF$_2$ unmix at higher temperatures than the isomeric C_4mimNTF$_2$, which may result from an additional, stabilizing contribution due to interactions of the acidic proton of the imidazolium ion of C_4mimNTF$_2$ with the alcohol solvent [74].

In order to compare the behaviour of the real solutions with that of the RPM, we show in figure 10(b) the critical temperatures in the RPM scale as a function of the dielectric permittivity. We have included data of solutions of $C_n$mimBF$_4$ ionic liquids (C_6mimBF$_4$, C_4mimBF$_4$) in alcohols (n-propanol, n-butanol, n-pentanol, n-hexanol, n-octanol, 2-pentanol, 2-butanol, i-butanol, t-butanol) (♦) [69, 74] and of C_{12}mimCl in benzene, toluene, o-xylene and tetralin and C_{14}mimCl in CCl_4 (■) [71]. The parameters describing the phase diagrams of ionic liquids with the anions BF_4^- and Cl^- are given in the tables of the appendix. For the transformation of the data into the RPM variables we take for the BF_4^- salts the maximum of the pair correlation function at 5.0 Å obtained in the simulation [91] as the figure for the hard-sphere diameter σ in the RPM. Other simulations of C_4mimBF$_4$ and C_2mimBF$_4$ yielded a similar figure of 4.9 Å [102]. If the data would agree exactly with the RPM, the critical temperatures of all systems should assume the same value T_c^*. The long dashed line gives the result of the simulations using FSS techniques. The short dashed line is the prediction of the FL mean-field model. In the scale of this plot the difference between the simulations and the mean-field model is marginal. The data for the non-polar solvents collapse into one point in this diagram to a value somewhat below the RPM value. For the solutions in the alcohols an almost linear increase of the critical temperatures T_c^* with the dielectric permittivity ε_c is found instead of a constant value of T_c^*. The increase of T_c^* with ε_c for the solutions in alcohols is opposite to the trend of T_c in the normal K temperature scale. The master plot includes the data of the non-polar solvents and would also include data for solutions in water, which are outside the range shown here. The correlation between T_c^* and ε was reported in earlier work [69–71] for the anions BF_4^-, PF_6^- and Cl^-. Because the RPM is an exact model only for $\varepsilon = 1$ [103], we draw also a line (dotted line) that would result if the RPM critical temperature is multiplied by ε_c. The observed correlation is between those two lines, which shows that the linear dependence of T_c^* on ε_c is not trivially caused by the RPM scaling. At present there is no theory available that can explain the empirical correlation. However, simulations on mixtures of charged hard spheres and hard-sphere dipoles state an increase of T_c^* with ε [104].

Now we have a closer look at the critical temperatures of the solutions in the non-polar solvents. As can be seen in figures 10(a) and 11(a), no correlation of T_c or T_c^* with the dielectric permittivity ε_c of the solvent can be found. Figure 11 compares the solutions of C_8mimNTF$_2$ in benzene and α-styrene (□), C_{10}mimNTF$_2$ in benzene, toluene and α-styrene (◊) [77] and C_{18}mimNTF$_2$ methylcyclohexane, cyclohexane and decalin (△). We have also included the data for solutions of C_{12}mimCl in benzene, toluene, o-xylene and tetralin (■) and CCl_4 (★) [71] in figure 11. For the RPM diameter of C_{12}mimCl the value of the maximum of the anion–cation radial distribution function of C_2mimCl of the simulations [91] is used, which is 4.6 Å in agreement with neutron scattering experiments [105] yielding 4.5 Å but above the figure of another simulation [106] yielding 4.0 Å. In our former analysis we used an even smaller value of 3.8 Å [69, 71] which was based on the crystal structure. Again, the solvents to the same salt are listed in the order of increasing critical temperatures. Figure 11(a) shows no correlation between T_c^* and the dielectric permittivity of the solvent; obviously the dielectric permittivity is not an appropriate parameter for rationalizing the differences of the critical temperatures in the solutions in non-polar solvents. Other properties such as the work required to separate the solvent molecules to form a solution may be more relevant. We take the boiling temperatures of the solvents as a measure of the strength of the solvent–solvent interactions. Figure 11(b) shows that for the same IL the figures of T_c^* increase with the boiling temperatures of the solvents taken from [107]. Comparing T_c^* for different ILs and the same solvent we observe a trend to decrease with the length of the side chain of the imidazolium anion. Thus the solvent–solvent interactions modify the transition temperatures in non-polar solvents, which are certainly determined by the Coulomb interactions. The critical temperatures T_c^* increase with the boiling temperature of the solvents, because

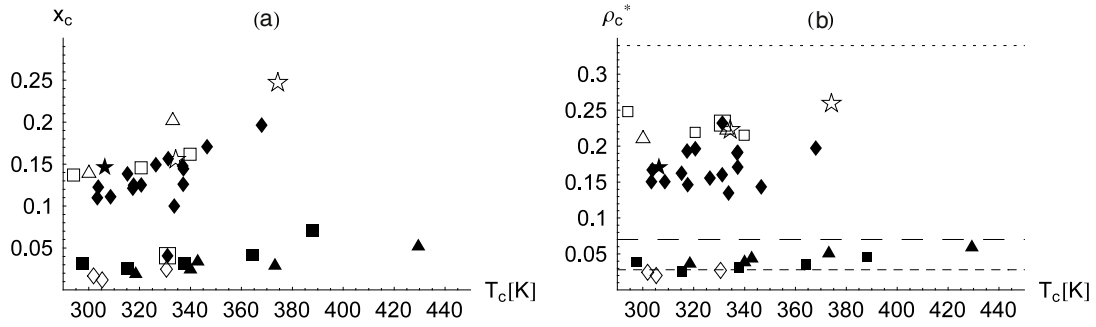

Figure 12. (a) Critical mole fraction and (b) critical RPM density as a function of the critical temperature. The long dashed line is the result of the simulations of the RPM, the short dashed line is the result of the Fisher–Levine theory and the dotted line gives the density of the Lennard-Jones system. The systems are labelled as in figure 10.

the strength of the solvent–solvent interactions reduces the stability of the mixtures. The longer side chain provides additional contributions of dispersive interactions with the solvent that stabilize the solution and hence reduce the separation temperatures.

3.2.2. Critical densities. Having analysed the critical temperatures we turn to a discussion of the critical compositions. The proper choice of the concentration variable in the analysis of the phase diagrams using the Wegner expansion or the crossover theory is a topic of long-standing discussion [53, 92]. We will not go into this matter but investigate if different choices of the variables may highlight certain correlations for groups of compounds that are similar from the physical–chemical point of view. In figures 12(a) and (b) we compare the critical compositions given as mol fraction x and as RPM density ρ^*, respectively. The densities are estimated assuming additive molar volumes. The densities of the solvents are taken from [97], while the densities of the NTF_2-ILs are taken from [108]. For reference on the densities of the ILs with the ions BF_4^- and Cl^- see [71, 69]. We see two groups of data, one for the solutions in alcohols, the other for the solutions in non-polar solvents. The critical compositions of the alcohol solutions are larger than those of the solutions in hydrocarbons and arenes. For the alcohol solutions the critical mole fractions (figure 12(a)) show a trend to increase with separation temperature. The critical concentration of the solution of C_6mimBF_4 in water (diamond in square), however, is in the region of the non-polar solvents, which is unreasonable. This discrepancy is removed when using the RPM density as the variable of the composition. With the RPM density as the concentration variable (figure 12(b)) the critical composition of the solution in water is in the region of the alcohols, which is reasonable. The critical densities show no trend. However, the scatter of the data among the protic solvents is rather large if compared to the representation in terms of the mole fraction. The figures for the solutions of the ILs with the NTF_2 anion are somewhat above that of the solutions of ILs with the BF_4^- anion.

An advantage of using the RPM density is that it enables us to compare with the theoretical and simulation results of the RPM and of the Lennard-Jones fluid. All critical densities are smaller than the critical density of the Lennard-Jones fluid (dotted line). The critical densities of the solutions in protic solvents are above that of the RPM (long dashed line) and below that for the solutions in aprotic solvents. Surprisingly, the RPM densities of the solutions in the aprotic solvents agree rather well with the result predicted by the FL theory [2, 42] (short dashed line), which may be fortuitous.

3.2.3. Width of phase diagrams. The next steps in the discussion concern the shape of the phase diagrams. In figures 13 we compare the width parameters b of the phase diagrams and the parameters B of the corresponding states representations for the various choices of the concentration variables, namely the molar fraction (figures 13(a) and (b)) and the RPM density ρ^* (figures 13(c) and (d)). Figures 13(e) and (f) show the width parameter of the phase diagrams represented in terms of the RPM variables T^* and ρ^*. The symbols of the data points have the same meaning as in figures 10 and 12. The width parameters b_x, b_ρ for the alcohol solutions are larger than that for the solutions in aprotic solvents. If the mol fraction is chosen as the variable, the width of the phase diagrams of the solution of C_6mimBF_4 in water is in the region of the aprotic solvents, while it is in the region of the alcohol solutions, when the RPM density is chosen as the variable of the composition. Thus we conclude again that the RPM density is a more appropriate variable of the composition than the mole fraction.

The difference between the solutions in alcohols and non-polar solvents vanishes in the corresponding state representations shown in figures 13(b) and (d), indicating a correlation of the parameters b with the critical compositions. The widths of the corresponding state diagrams based on the RPM density in the solutions in protic and aprotic solvents are very similar, with values near the simulation result of the RPM (long dashed) and mostly below the figure of the FL theory (short dashed). The dotted line in figure 13(d) is the width of the corresponding state phase diagrams of the Lennard-Jones fluid, which is smaller than that of the ionic solutions.

A substantial difference (figures 13(e) and (f)) between the width parameters of the phase diagrams of the solutions in protic and aprotic solvents results if both the density and the temperature are expressed in the RPM scales. Then, due to the temperature dependence of the dielectric permittivity of the solvents, the UCSPs observed for the solutions in the

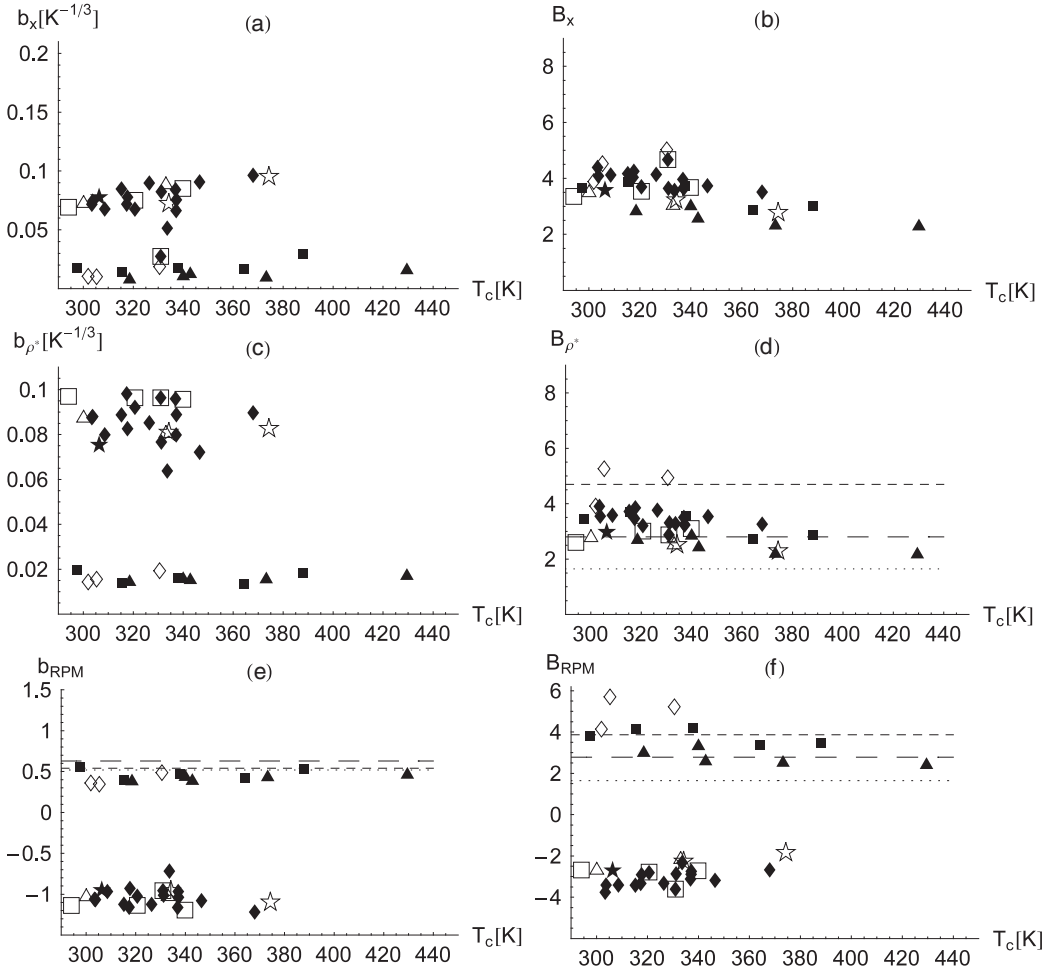

Figure 13. Widths of the phase diagrams with (a) the mole fraction and (c) the RPM density as concentration variable; (e) gives the widths when the phase diagrams are represented in terms of the RPM variables; (b), (d) and (f) give the widths for the corresponding state diagrams. The systems are labelled as in figure 10, while the lines represent the same calculations as in figure 12.

protic solvents become LCSPs and hence the width parameter becomes negative. The critical points of the non-polar solvents remain UCSPs. The absolute values of b_{RPM} of the phase diagrams in aprotic solvents are smaller than that of the solutions in protic solvents (figure 13(e)). Within the two groups of solutions the scatter of the values of the parameter b_{RPM} is remarkably small. The values of the width parameters b_{RPM} of the phase diagrams concerning aprotic solvents are only a little smaller than the RPM value (long dashed line). The agreement with the values obtained from the FL theory (short dashed line) and the Lennard-Jones fluid (dotted line) is even better. The representation of the phase diagrams in terms of the RPM variables appears to be the best.

In the corresponding state representation (figure 13(f)) based on the RPM variables the absolute values of B_{RPM} are similar for the groups of the solutions in protic and aprotic solvents. The figures of the width parameters of ionic solutions in the aprotic solvents are in the region predicted by the simulations of the RPM (long dashed line) and the prediction of the Fisher–Levin mean-field theory (short dashed line) and above that of the Lennard-Jones fluid. The scatter of the data points concerning the solutions in the non-polar solvents is larger if compared to the representation in unscaled RPM variables. Note that the reduced variables $(\rho^* - \rho_c^*)/\rho_c^*$ and $(T_c^* - T^*)/T_c^*$ are invariant against the choice of the separation σ. If the RPM temperatures would be calculated just taking the dielectric permittivity of the solvent at the critical temperature, the corresponding state temperatures calculated from the conventional Kelvin scale would be identical with that calculated on the basis of the RPM temperatures.

3.2.4. Asymmetry of the phase diagrams. It remains to discuss the slopes a and A of the diameter visualized in figures 14(a)–(f).

The scatter of the data is much larger than for the other parameters. Comparing the figures for the protic and aprotic solvents with the molar fraction as variable (figure 14(a)) the asymmetry is seen to be larger for the solutions in alcohols. Exceptions are the phase diagrams of C_{18}mimNTF$_2$ in cyclohexane, methylcyclohexane and decalin, with a slope which is in the region found for the alcohol solutions. With the RPM density as concentration variable (figure 14(c)) the difference of the asymmetry of the phase diagrams in protic and aprotic solvents becomes smaller. Using the corresponding state variables (figures 14(b) and (d)) the difference between the asymmetry of the phase diagrams between protic and

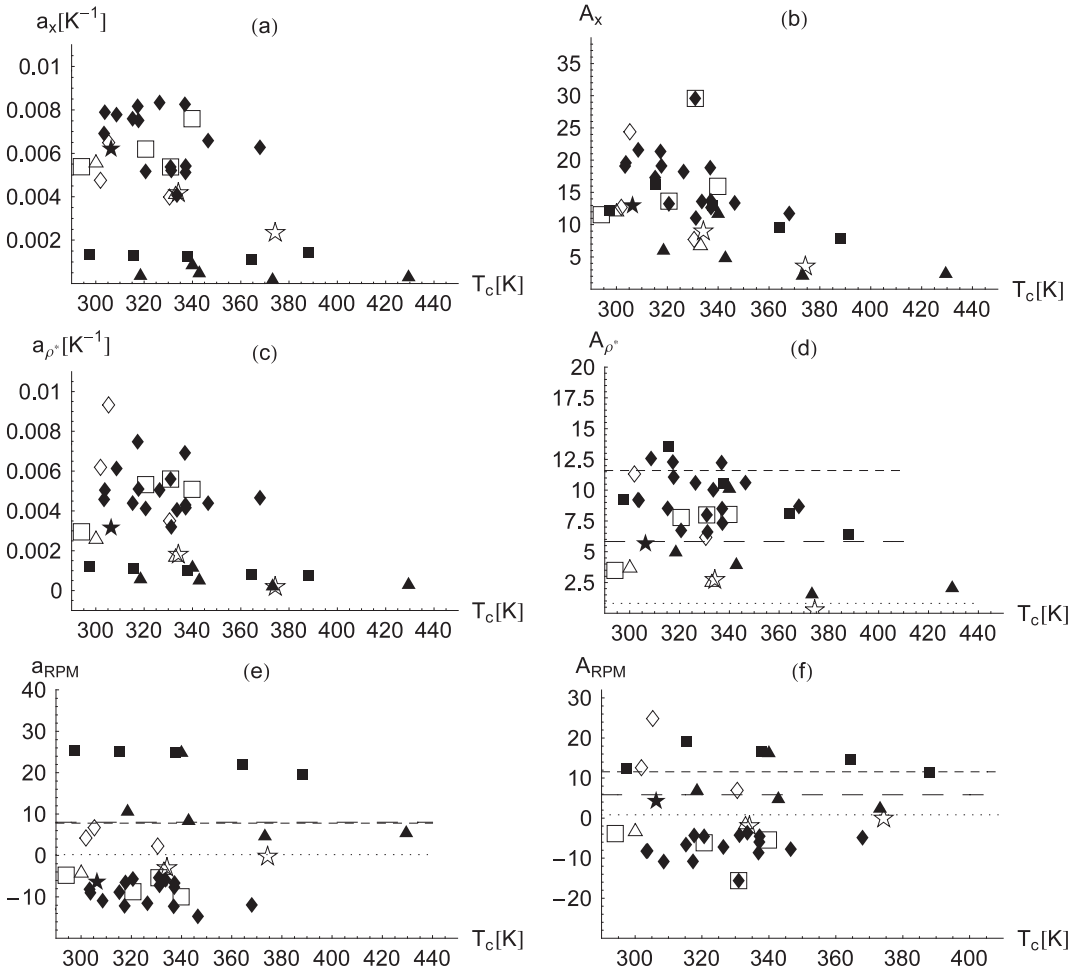

Figure 14. Slope of the diameter of the phase diagrams with (a) the mole fraction and (c) the RPM density as concentration variable; (e) gives the slope of the diameter when the phase diagrams are represented in terms of the RPM variables. The figures (b), (d) and (f) concern the corresponding state diagrams. The systems are labelled as in figure 10, while the lines are as in figure 12.

aprotic solvents vanishes for both variables. Most data are between the figure obtained for the RPM and the FL theory and above that of the Lennard-Jones fluid. The scatter of the data points is too large to allow further conclusions.

At last we discuss the slope of the diameter for the phase diagrams using both the RPM variables (figure 14(e)). Because the UCSP of the phase diagrams of the ionic solutions in alcohols become LCSP, when using the RPM variables, the slope parameter of the diameter of the phase diagrams becomes negative. While the data for the alcohol solutions are fairly similar for different anions, this is not the case for the data concerning the solutions in aprotic solvents: for the solutions of ILs with the NTF_2 anion the slope of the diameter is near the RPM value, while the corresponding values for the solution of the ILs with the Cl^- anion are much larger. This picture is changed only a little when using the corresponding states variables (figure 14(f)). The absolute values of the slope of the diameter of the solutions in protic and aprotic solvents are rather similar. The asymmetry of the corresponding state phase diagrams of the solutions of the ILs with the NTF_2^- anion in aromatic solvents is near that of the RPM. The asymmetry of the phase diagrams of the solutions of the ILs with the Cl^- anion is even larger than calculated by the FL theory [71, 95].

To close this discussion we show in figure 15 the corresponding state phase diagrams of the IL solutions in alcohols (figure 15(a)) and in non-polar solvents (figure 15(b)) based on the RPM variables. The phase diagrams of the solutions in alcohols have a LCSP and most of them follow closely a master plot. Noticeable deviations are the solutions of C_3mmimNTF$_2$ in hexanol (☆) with a much smaller asymmetry and of C_6mimBF$_4$ in water, where the asymmetry is larger than for other solutions. The phase diagrams in non-polar solvents all have a UCSP. The asymmetry for the Lennard-Jones fluid is almost not noticeable in the figure. The phase diagrams of C_8mimNTF$_2$ in benzene are less asymmetric than the RPM (long dashed line), while the asymmetry of the phase diagrams of the solutions of $C_n$mimCl is bigger. Particularly large is the asymmetry of the solutions of C_{18}mimNTF$_2$ in hydrocarbons. According to the numerical analysis of the phase diagrams given above the differences of the various corresponding state plots are mainly caused by the diameter, while the width is rather similar for all systems.

4. General discussion

The aim of this paper is the comparison of the phase diagrams of real ionic solutions in polar and non-polar solvents with

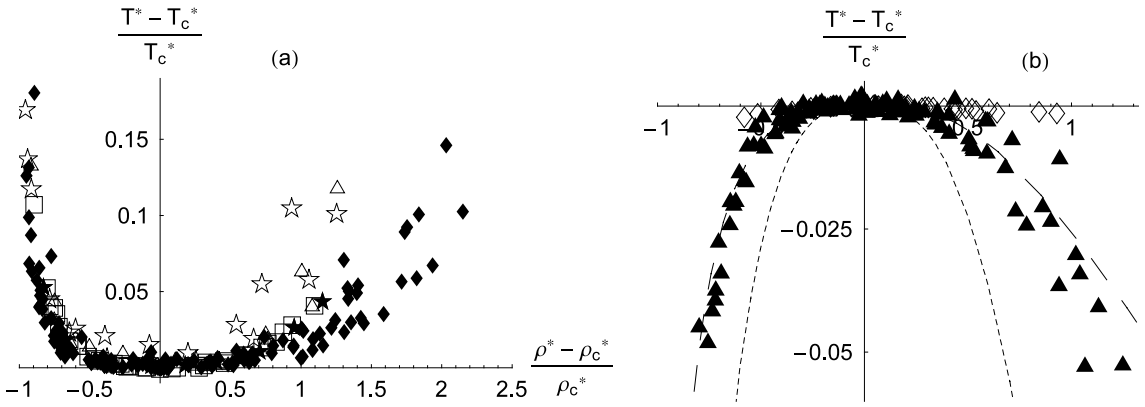

Figure 15. Corresponding state phase diagrams of ionic solutions in (a) alcohols and (b) non-polar solvents based on data expressed by the RPM variables. Labelling of the systems is identical to that of figure 10. The long dashed line is the fit to the simulation results of the RPM, while the dotted line represents the Lennard-Jones fluid.

model systems of ionic fluids, the primitive model and the restricted primitive model. It is understood that the model fluids RPM and PM can only be regarded as cartoons of the real ionic solutions, describing the Coulomb part of the interactions. The analysis uses corresponding state considerations as a tool in the discussion of the phase diagrams, having in mind that the principle of the corresponding state with its very strong conditions cannot be expected to apply in a rigorous manner.

We have reported the first liquid–liquid phase diagrams of an ionic solution in cyclohexane, which is the prototype of an inert solvent, and in the cyclic hydrocarbons methylcyclohexane and decalin. It can be said that parameters of the phase diagrams reported in this work are in general agreement with those observed for other ionic solutions in non-polar solvents.

The data of the model systems and of the real solutions are both analysed applying simplified scaling laws that presume Ising criticality and (with the exception of the solutions of C_{18}mimNTF_2 in cyclic hydrocarbons) the heuristic validity of the rectilinear diameter rule.

The analysis is carried out using the mole fraction and the RPM density as variables of the composition. The data are also analysed in terms of the RPM variables.

In the primitive model, which allows different sizes of the charged hard spheres all properties such as the critical temperature, the critical density, the width of the phase diagrams and also the slope of the diameter decrease with the increasing difference of the size of the ions. Using corresponding state variables, the relative changes of the parameters describing the shape of the diagrams are reduced.

We have analysed phase diagrams of solutions of ionic liquids with imidazolium cations differing in the length of the side chain, and the anions Cl^-, BF_4^- and NTF_2^- that differ in size. The anions Cl^- and BF_4^- can be reasonably well regarded as spherical, which is not so for the NTF_2^- ion, which has a complicated shape and forms two conformers. The solvents were hydrocarbons, arenes and alcohols. For the analysis in terms of the RPM variables it is assumed that the charge of the imidazolium cation is centred at the imidazolium ring so that the cations of the considered ILs are regarded as equal-sized although the size of the cations varies substantially with the length of the side chain. The maximum of the anion–cation pair correlation function, which concerns the mass centres of the imidazolium ring and of the anion obtained by simulations, is taken as the distance of the charges at contact of the ions when expressing the phase diagrams in terms of the RPM variables. In former work rather ad hoc estimates of the charge separation at contact based on simple estimates using van der Waals radii and bond lengths were used, which were not appropriate for dealing with the NTF_2 anion. The choice of the maxima of the cation–anion pair distribution function as the diameter σ in the RPM allowed a consistent representation of the phase diagrams of the solutions of ILs with the anions Cl^-, BF_4^- and NTF_2^-. The data of the ILs with different anions show the same behaviour if they are represented in RPM variables. The observation that the parameters of the phase diagrams do not depend on the lengths of the side chains corroborates the model that the liquid–liquid phase transition is mainly determined by the Coulomb part of the ILs.

The variation of the relative size of the anions and of the cations is too small to show the variation of the properties obtained in the simulations of the primitive model. The influence of the solvent, which has not yet been treated adequately, seems to be more important. The critical density and the critical temperature as well as the parameters of the width and the slope of the diameter allow a clear distinction between the solutions in alcohols including water and the solutions in non-polar solvents. While in the non-polar solvents the critical temperatures do not depend on the dielectric permittivity of the solvent, they are reduced in alcohols with increasing dielectric permittivity of the solvents. In the RPM temperature scale the critical temperatures are located on a master plot, which shows an essentially linear increase with the dielectric permittivity of the solvents including hydrocarbons and water. While the critical temperatures of the ionic solutions in polar solvents are larger than the RPM value, they are smaller for solutions in non-polar solvents and are located at the same position in the scale of this plot. A finer analysis shows a correlation of the RPM critical temperatures of the ionic solutions in non-polar solvents with the boiling temperatures of the solvents. The critical

temperatures T_c^* increase with the boiling temperature of the solvents, as the strength of the solvent–solvent interactions reduces the stability of the mixtures. The longer side chain provides additional contributions of dispersive interactions with the solvent, which stabilize the solution and hence reduce the separation temperatures. Thus the solvent–solvent interactions modify the transition temperatures in non-polar solvents, which are certainly determined by the Coulomb interactions.

The critical compositions are different for the solutions in alcohols and non-polar solvents but do not vary with the dielectric permittivity of the solvents. The critical densities of the solutions in alcohols are above the RPM value and below that figure in non-polar solvents. With the mole fraction as variable the critical compositions of the ionic solutions in water are in the region of the solutions in the aprotic solvents, while the analyses based on the RPM density locates the critical densities of the water solutions among the alcohols, which appears more reasonable. Furthermore, the critical mol fractions increase with the critical temperatures of the solutions, while the data based on analyses in terms of the RPM density show no systematic change. In other words: the number density of the ions determines the critical composition.

The analysis of the shape of phase diagrams leads to similar conclusions. Both the width and the asymmetry of the phase diagrams of the solutions in the protic solvents are larger than in the aprotic solvents. Again, the data of the width of the solutions in water are in the region of the non-polar solvents if the mol fraction is the variable of the composition, but agree with the data found for the alcohol solutions if the RPM density is chosen. In the corresponding state diagrams the difference between the width parameters of the phase diagrams in protic and aprotic solvents vanishes. This is also true for the slope of the diameter which determines the asymmetry of the phase diagrams. While the width is rather similar for all systems, the scatter of the values obtained for the diameter is larger: the differences between the corresponding state plots are mainly caused by the diameter.

The analyses based on the phase diagrams represented in terms of the RPM variables leads to a remarkable result. In this representation all phase diagrams of the solutions in alcohols and water get an LCSP. The parameters of the phase diagrams with the solutions in protic and aprotic solvents are distinguished by the sign and show now further systematic changes. Thus, the analysis in terms of the RPM variables allows a clear distinction between the ionic solutions in protic and aprotic solvents.

In the data analysis we have mostly applied the simplified scaling relations equations (4) and (5). It is now known that the rectilinear linear diameter rule is incorrect: non-analytic contributions determine the diameter when approaching the critical temperature [54–57]. Fits assuming the rectilinear diameter lead to different slopes of the diameter, when changing the temperature range included into the fit. In fact, the phase diagrams of the solutions of C_{18}mimNTF$_2$ in cyclohexane, methylcyclohexane and tetralin were measured only in a small temperature range of about 1 K. Presuming the applicability of the rectilinear diameter rule led to a slope of the diameter which appeared unrealistically large so that we assumed that in those cases the 2β term of the expansion equation (3) may determine the asymmetry.

In part the scatter of the slope of the diameter in the two solvent groups, which is larger than for the other parameters, may be due to the simplifying assumption of the rectilinear diameter. A further reason may be that the coefficients determining the temperature dependence of the diameter are differences of combinations of higher terms in the Landau–Ginzburg expansion and hence may be particularly sensitive to details of the intermolecular potentials [71, 95]. It is quite likely that data of higher accuracy that allow using the accurate scaling relations may allow identifying subtle correlations. Unfortunately, the accuracy of the data and the number of data points available for this analysis did not allow an analysis in accordance with the modern developments of the theory of critical phenomena such as the crossover theory [45] and the complete scaling [54–57]. Work on very few systems that hopefully have the required accuracy is carried out at present.

Most liquid–liquid phase transitions in ionic solutions are in accordance with the results of the analysis given in this paper. However, there are reports of experiments that may challenge the generality of our considerations. LCSPs have been observed repeatedly in ionic solutions [21, 80, 81, 88]. It was demonstrated in former work [71] that phase diagrams in aprotic solvents including the KI/SO_2-system and solutions of the salt trimethyl-ethylammonium iodide (N_{1112}I) [21] in chloroform that have an LCSP get a UCSP when using the RPM variables and taking the temperature dependence of the dielectric permittivity of the solvent into account so that agreement with the behaviour expected for ionic solution in aprotic solvents can nevertheless be stated. Closed solubility loops and LCSPs that are observed in ionic solutions in water have been explained as a consequence of the breaking of the hydrogen bond network with increasing temperature [58, 109]. Such explanations, however, are not appropriate if considering the LCSPs reported for ionic solutions in arenes [77, 87]. Specific interactions between the arenes and the ions leading to clathrate-like structures [110] may be important in such cases. Alternatively, it may well be that the RPM or simple ionic solutions when investigated at lower temperatures than considered until now in theory and simulations may lead to closed loop phase diagrams. One could speculate that at low temperatures non-polar associates such as quadrupoles may be solved better than the ion pairs and free ions, and aggregation of the ions may break with rising temperature.

In conclusion we state the need of theoretical and simulation work on the phase transitions of ionic solutions that may provide the explanations of the correlations found in the empirical analysis reported in this paper.

Acknowledgments

This work was supported by grant SCHR188/10-1 of the Deutsche Forschungsgemeinschaft in the SSP ‘Ionic Liquids’. Drs J Köser, D Sarcsan, V C Weiss and B Rathke are thanked for their support and discussions. Special thanks go to Professor A Z Panagiotopoulos for providing the unpublished data of the phase diagrams of the primitive model.

Appendix

Table A.1. Parameters of the phase diagrams of imidazolium ionic liquids with the BF_4^- and the Cl^- anion represented with the mole fraction as a variable of the composition.

System	T_c (K)	x_c	b_x ($K^{-1/3}$)	a_x (K^{-1})	B_x	A_x	ε_c	Reference
C_6mimBF_4/H_2O	330.98	0.041	0.027	0.0054	4.67	29.58	67.40	[69]
C_6mimBF_4/C_3OH	287.71	0.102	0.067	0.0098	4.37	27.76	21.75	[69]
C_6mimBF_4/C_4OH	303.73	0.122	0.074	0.0079	4.08	19.59	16.56	[69]
C_6mimBF_4/C_5OH	315.24	0.138	0.085	0.0076	4.17	17.30	12.63	[69]
C_6mimBF_4/C_6OH	326.41	0.149	0.090	0.0083	4.14	18.22	9.84	[69]
C_6mimBF_4/2-C_5OH	317.67	0.125	0.078	0.0075	4.25	19.13	10.20	[69]
C_6mimBF_4/2-C_4OH	303.40	0.110	0.072	0.0069	4.39	19.10	16.60	[69]
C_4mimBF_4/C_3OH	317.34	0.121	0.072	0.0082	4.04	21.35	17.88	[74]
C_4mimBF_4/i-C_3OH	320.63	0.125	0.068	0.0052	3.69	13.23	16.10	[74]
C_4mimBF_4/C_4OH	336.89	0.148	0.084	0.0083	3.96	18.83	13.10	[74]
C_4mimBF_4/2-C_4OH	337.14	0.126	0.066	0.0051	3.66	13.69	13.09	[74]
C_4mimBF_4/i-C_4OH	337.23	0.144	0.076	0.0054	3.65	12.65	12.72	[74]
C_4mimBF_4/t-C_4OH	333.60	0.100	0.051	0.0041	3.57	13.62	8.24	[74]
C_4mimBF_4/C_6OH	367.97	0.197	0.096	0.0063	3.51	11.75	7.21	[74]
C_6mimBF_4/C_4OH	308.58	0.111	0.068	0.0078	4.12	21.61	16.01	[74]
C_6mimBF_4/C_6OH	331.23	0.156	0.082	0.0052	3.64	11.05	9.49	[74]
C_6mimBF_4/C_8OH	346.52	0.171	0.091	0.0066	3.73	13.38	7.18	[74]
C_{12}mimCl/benz	297.45	0.032	0.0175	0.0013	3.65	12.27	2.27	[71]
C_{12}mimCl/tol	337.76	0.032	0.0172	0.0012	3.73	13.04	2.27	[71]
C_{12}mimCl/o-xyl	364.25	0.042	0.0167	0.0011	2.88	9.63	2.34	[71]
C_{12}mimCl/tetra	388.02	0.071	0.0292	0.0014	3.02	7.84	2.48	[71]
C_{14}mimCl/CCl4	315.40	0.025	0.0143	0.0013	3.88	16.22	2.19	[71]

Table A.2. Parameters of the phase diagrams of imidazolium ionic liquids with the BF_4^- and the Cl^- anion represented with the RPM density as a variable of the composition.

System	T_c (K)	ρ_c	b_ρ ($K^{-1/3}$)	a_ρ (K^{-1})	B_ρ	A_ρ	ε_c	Reference
C_6mimBF_4/H_2O	331.28	0.232	0.096	0.0056	2.87	7.99	67.30	[69]
C_6mimBF_4/C_3OH	287.71	0.168	0.094	0.0074	3.68	12.59	21.75	[69]
C_6mimBF_4/C_4OH	303.73	0.167	0.088	0.0050	3.55	9.18	16.56	[69]
C_6mimBF_4/C_5OH	315.23	0.162	0.089	0.0044	3.72	8.53	12.63	[69]
C_6mimBF_4/C_6OH	326.41	0.156	0.085	0.0050	3.77	10.59	9.84	[69]
C_6mimBF_4/2-C_5OH	317.66	0.146	0.083	0.0051	3.85	11.07	10.20	[69]
C_6mimBF_4/2-C_4OH	303.39	0.151	0.088	0.0046	3.90	9.22	16.60	[69]
C_4mimBF_4/C_3OH	317.41	0.193	0.098	0.0075	3.47	12.29	17.87	[74]
C_4mimBF_4/i-C_3OH	320.66	0.196	0.092	0.0041	3.21	6.73	16.10	[74]
C_4mimBF_4/C_4OH	337.02	0.191	0.096	0.0069	3.50	12.23	13.09	[74]
C_4mimBF_4/2-C_4OH	337.30	0.171	0.080	0.0043	3.25	8.50	13.06	[74]
C_4mimBF_4/i-C_4OH	337.30	0.192	0.089	0.0042	3.23	7.32	12.71	[74]
C_4mimBF_4/t-C_4OH	333.70	0.135	0.064	0.0041	3.28	10.04	8.23	[74]
C_4mimBF_4/C_6OH	368.03	0.197	0.090	0.0047	3.26	8.69	7.20	[74]
C_6mimBF_4/C_4OH	308.65	0.151	0.080	0.0061	3.58	12.57	16.00	[74]
C_6mimBF_4/C_6OH	331.22	0.160	0.077	0.0032	3.31	6.61	9.49	[74]
C_6mimBF_4/C_8OH	346.54	0.143	0.072	0.0044	3.53	10.61	7.18	[74]
C_{12}mimCl/benzene	297.45	0.039	0.020	0.0012	3.43	9.21	2.28	[71]
C_{12}mimCl/toluene	337.76	0.032	0.016	0.0010	3.57	10.58	2.25	[71]
C_{12}mimCl/o-xylene	364.24	0.035	0.014	0.0008	2.73	8.09	2.34	[71]
C_{12}mimCl/tetralin	388.00	0.046	0.018	0.0008	2.86	6.42	2.48	[71]
C_{14}mimCl/CCl_4	315.40	0.025	0.014	0.0011	3.72	13.57	2.19	[71]

Table A.3. Parameters of the phase diagrams of imidazolium ionic liquids with the BF_4^- and the Cl^- anion represented in the variables of the RPM.

System	T_c	ρ_c	b_{RPM}	a_{RPM}	B_{RPM}	A_{RPM}	ε_c	Reference
C_6mimBF_4/H_2O	0.6751	0.232	−0.96	−5.36	−3.61	−15.59	67.30	[69]
C_6mimBF_4/C_3OH	0.1894	0.168	−1.13	−12.92	−3.87	−14.54	21.75	[69]
C_6mimBF_4/C_4OH	0.1523	0.167	−1.07	−8.98	−3.41	−8.20	16.56	[69]
C_6mimBF_4/C_5OH	0.1206	0.162	−1.12	−8.87	−3.42	−6.59	12.63	[69]
C_6mimBF_4/C_6OH	0.0973	0.156	−1.13	−11.54	−3.32	−7.21	9.84	[69]
$C_6mimBF_4/2C_5OH$	0.0981	0.147	−0.93	−6.52	−2.91	−4.34	10.20	[69]
$C_6mimBF_4/2C_4OH$	0.1525	0.151	−1.06	−8.14	−3.76	−8.25	16.60	[69]
C_4mimBF_4/C_3OH	0.1718	0.194	−1.16	−12.18	−3.33	−10.80	17.87	[74]
$C_4mimBF_4/i\text{-}C_3OH$	0.1563	0.196	−1.03	−5.69	−2.81	−4.53	16.10	[74]
C_4mimBF_4/C_4OH	0.1336	0.191	−1.16	−12.28	−3.12	−8.61	13.09	[74]
$C_4mimBF_4/2\text{-}C_4OH$	0.1334	0.171	−0.97	−7.64	−2.89	−5.97	13.06	[74]
$C_4mimBF_4/i\text{-}C_4OH$	0.1298	0.192	−1.04	−6.65	−2.75	−4.52	12.71	[74]
$C_4mimBF_4/t\text{-}C_4OH$	0.0831	0.134	−0.72	−5.87	−2.33	−3.64	8.23	[74]
C_4mimBF_4/C_6OH	0.0803	0.196	−1.22	−11.93	−2.68	−4.88	7.20	[74]
C_6mimBF_4/C_4OH	0.1495	0.151	−0.97	−10.91	−3.41	−10.84	16.00	[74]
C_6mimBF_4/C_6OH	0.0952	0.161	−1.01	−7.19	−2.87	−4.26	9.49	[74]
C_6mimBF_4/C_8OH	0.0753	0.143	−1.08	−14.72	−3.18	−7.73	7.18	[74]
$C_{12}mimCl$/benzene	0.0189	0.039	0.55	25.41	3.79	12.42	2.27	[71]
$C_{12}mimCl$/toluene	0.0212	0.032	0.48	24.97	4.18	16.75	2.25	[71]
$C_{12}mimCl$/o-xylene	0.0237	0.036	0.42	22.05	3.39	14.72	2.34	[71]
$C_{12}mimCl$/tetraline	0.0268	0.046	0.53	19.51	3.46	11.32	2.48	[71]
$C_{14}mimCl/CCl_4$	0.0193	0.025	0.39	25.08	4.16	19.11	2.19	[71]

References

[1] Pitzer K S 1990 *Acc. Chem. Res.* **23** 333
[2] Fisher M E 1994 *J. Stat. Phys.* **75** 1
[3] Stell G 1995 *J. Stat. Phys.* **78** 197
[4] Anisimov M A 1991 *Critical Phenomena in Liquids and Liquid Crystals* (Philadelphia: Gordon and Breach)
[5] Domb C 1996 *The Critical Point* (London: Taylor and Francis)
[6] Guggenheim E A 1945 *J. Chem. Phys.* **13** 253
[7] Buback M and Franck E U 1972 *Ber. Bunsenges. Phys. Chem.* **76** 350
[8] Singh R R and Pitzer K S 1990 *J. Chem. Phys.* **92** 6775
[9] Zhang K C, Briggs M E, Gammon R W and Levelt Sengers J M H 1992 *J. Chem. Phys.* **97** 8692
[10] Wiegand S, Briggs M E, Levelt Sengers J M H, Kleemeier M and Schröer W 1998 *J. Chem. Phys.* **109** 9038
[11] Wiegand S, Levelt Sengers J M H, Zhang K J, Briggs M E and Gammon R W 1997 *J. Chem. Phys.* **106** 2777
[12] Schröer W, Wagner M and Stanga O 2006 *J. Mol. Liq.* **127** 2
[13] Wiegand S, Berg R F and Levelt Sengers J M H 1998 *J. Chem. Phys.* **109** 4533
[14] Kleemeier M, Wiegand S, Derr T, Weiss V, Schröer W and Weingärtner H 1996 *Ber. Bunsenges. Phys. Chem.* **100** 27
[15] Oleinikova A and Bonetti M 1996 *J. Chem. Phys.* **104** 3111
[16] Wagner M, Stanga O and Schröer W 2004 *Phys. Chem. Chem. Phys.* **6** 1750
[17] Kleemeier M, Wiegand S, Schröer W and Weingärtner H J 1999 *J. Chem. Phys.* **110** 3085
[18] Oleinikova A and Bonetti M 1999 *Chem. Phys. Lett.* **299** 417
[19] Wagner M, Stanga O and Schröer W 2004 *Phys. Chem. Chem. Phys.* **6** 4421
[20] Schröer W, Wiegand S and Weingärtner H 1993 *Ber. Bunsenges. Phys. Chem.* **97** 975
[21] Wiegand S, Kleemeier M, Schröder J M, Schröer W and Weingärtner H 1994 *Int. J. Thermophys.* **15** 1045
[22] Bonetti M, Bagnuls C and Bervillier C 1997 *J. Chem. Phys.* **107** 550
[23] Schröer W, Kleemeier M, Plikat M, Weiss V and Wiegand S 1996 *J. Phys.: Condens. Matter* **8** 9321
[24] Barthel J, Carl E and Gores H J 1999 *Electrochem. Solid State Lett.* **2** 218
[25] Weingärtner H, Merkel T, Maurer U, Conzen J-P, Glassbrenner H and Käshammer S 1991 *Ber. Bunsenges. Phys. Chem.* **95** 1579
[26] Weingärtner H, Wiegand S and Schröer W 1991 *J. Chem. Phys.* **96** 848
[27] Narayanan T and Pitzer K S 1994 *J. Phys. Chem.* **98** 9170
[28] Caillol J-M, Levesque D and Weiss J-J 2002 *J. Chem. Phys.* **116** 10794
[29] Orkoulas G and Panagiotopoulos A Z 1999 *J. Chem. Phys.* **110** 1581
[30] Yan Q L and de Pablo J J 1999 *J. Chem. Phys.* **111** 9509
[31] Romero-Enrique J M, Orkoulas G, Panagiotopoulos A Z and Fisher M E 2000 *Phys. Rev. Lett.* **85** 4558
[32] Yan Q L and de Pablo J J 2001 *Phys. Rev. Lett.* **86** 2054
[33] Yan Q L and de Pablo J J 2002 *Phys. Rev. Lett.* **88** 095504
[34] Panagiotopoulos A Z and Fisher M E 2002 *Phys. Rev. Lett.* **88** 045701
[35] Kim Y C and Fisher M E 2004 *Phys. Rev. Lett.* **92** 185703
[36] Panagiotopoulos A Z 2005 *J. Phys.: Condens. Matter* **17** S3205
[37] Panagiotopoulos A Z 1992 *Fluid Phase Equilib.* **76** 97
[38] Caillol J M 1994 *J. Chem. Phys.* **100** 2161
[39] Orkoulas G and Panagiotopoulos A Z 1994 *J. Chem. Phys.* **101** 1452
[40] Debye P and Hückel E 1923 *Physik. Z* **24** 185
[41] Fisher M E and Levin Y 1993 *Phys. Rev. Lett.* **71** 3826
[42] Levin Y and Fisher M E 1996 *Physica* A **225** 164
[43] Ebeling W 1971 *Z. Phys. Chem. (Lpz.)* **247** 340
[44] Aqua J-N, Banerjee S and Fisher M E 2005 *Phys. Rev.* E **72** 041501
[45] Anisimov M A and Sengers J V 2000 The critical region *Equations of State for Fluids and Fluid Mixtures* ed J V Sengers, R F Kayser, C J Peters and H J White (Amsterdam: Elsevier)
[46] Leote de Carvalho R J F and Evans R 1995 *J. Phys.: Condens. Matter* **7** L575
[47] Lee B P and Fisher M E 1996 *Phys. Rev. Lett.* **76** 2906
[48] Schröer W and Weiss V C 1998 *J. Chem. Phys.* **109** 8504
Schröer W and Weiss V C 1999 *J. Chem. Phys.* **110** 4687 (erratum)

[49] Kulinskii V L and Malomuzh N P 2003 *Phys. Rev.* E **67** 011501
[50] Patshan O V, Caillol J-M and Mryglod I M 2007 *Eur. Phys. J.* B **58** 449
[51] Narayanan T and Pitzer K S 1995 *J. Chem. Phys.* **102** 8118
[52] Gutkowski K, Anisimov M A and Sengers J V 2001 *J. Chem. Phys.* **114** 3133
[53] Ley-Koo M and Green M S 1981 *Phys. Rev.* A **23** 2650
[54] Kim Y C, Fisher M E and Orkoulas G 2003 *Phys. Rev.* E **67** 061506
[55] Wang J and Anisimov M A 2007 *Phys. Rev.* E **75** 051107
[56] Cerdeiriña C A, Anisimov M A and Sengers J V 2006 *Chem. Phys. Lett.* **424** 414
[57] Wang J, Cerdeiriña C A, Anisimov M A and Sengers J V 2008 *Phys. Rev.* E **77** 031127
[58] Weingärtner H, Kleemeier M, Wiegand S and Schröer W 1995 *J. Stat. Phys.* **78** 169
[59] Weingärtner H and Schröer W 2001 *Adv. Chem. Phys.* **116** 1
[60] Levelt Sengers J M H, Harvey A H and Wiegand S 2000 *Equations of State for Fluids and Fluide Mixtures* ed J V Sengers, R F Kayser, C J Peters and H J White (Amsterdam: Elsevier) p 805
[61] Wasserscheid P and Keim W 2000 *Angew. Chem. Int. Edn* **39** 3772
[62] Rogers R D and Seddon K R (ed) 2002 *Ionic Liquids: Industrial Applications for Green Chemistry* (*ACS Symposium* vol 818) (Oxford: Oxford University Press)
[63] Rogers R D and Seddon K R (ed) 2003 *Ionic Liquids as Green Solvents—Progress and Prospects* (*ACS Symposium* vol 856) (Oxford: Oxford University Press)
[64] Holbrey J D and Seddon K R 1999 *J. Chem. Soc. Dalton Trans.* 2133
[65] Zaitsau D H, Kabo G J, Strechan A A, Paulecka Y U, Tschersich A, Verevkin S V and Heintz A 2006 *J. Phys. Chem.* A **110** 7303
[66] Rebelo L P, Canognia Lopes J N, Esperanca J M S S and Filipe E 2005 *J. Phys. Chem.* B **109** 6040
[67] Zaitsau D H, Paulechka Y U and Kabo G J 2006 *J. Phys. Chem.* A **110** 11602
[68] Weingärtner H 2008 *Angew. Chem. Int. Edn* **47** 654
[69] Wagner M, Stanga O and Schröer W 2003 *Phys. Chem. Chem. Phys.* **5** 3943–50
[70] Saracsan D, Rybarsch C and Schröer W 2006 *Z. Phys. Chem.* **220** 1417
[71] Butka A, Vale V R, Saracsan D, Rybarsch C, Weiss V C and Schröer W 2008 *Pure Appl. Chem.* **80** 1613
[72] Marsh K N, Deev A V, Wu C-T, Tran E and Klamt A 2002 *Korean J. Chem. Eng.* **19** 357
[73] Wu C-T, Marsh K N, Deev A V and Boxall J A 2003 *J. Chem. Eng. Data* **48** 486
[74] Crosthwaite J M, Aki S N V K, Maginn E J and Brennecke J F 2004 *J. Phys. Chem.* B **108** 5113
[75] Heintz A, Lehmann J and Wertz C 2003 *J. Chem. Eng. Data* **48** 472
[76] Domanska U, Zolek-Tryznowska Z and Krolikowski M 2008 *J. Solut. Chem.* **37** 1271
[77] Lachwa J, Szydlowski J, Makowska A, Seddon K R, Esperanca J M S S, Guedesaand H J R and Rebelo L P N 2006 *Green Chem.* **8** 262
[78] Domanska U and Casas L M 2007 *J. Phys. Chem.* B **111** 4109
[79] Domanska U and Paduszynski K 2008 *J. Phys. Chem.* B **112** 11054
[80] Lachwa J, Szydlowski J, Naidanovic-Visac V, Rebelo L R N, Seddon K R, Nunes da Pont M, Esperanca J M S S and Guedes H J R 2005 *J. Am. Chem. Soc.* **127** 6542
[81] Shiflett M B and Yokozeki A 2006 *J. Phys. Chem.* B **110** 14436
[82] Hirschfelder J O, Curtis C F and Bird R B 1964 *Molecular Theory of Gases and Liquids* (New York: Wiley)
[83] Schröer W 2006 *J. Mol. Liq.* **125** 164
[84] Dittmar H, Butka A, Vale V R and Schröer W 2009 *J. Mol. Liq.* **145** 116
[85] Weiss V C and Schröer W 2005 *J. Chem. Phys.* **122** 084705
[86] Weiss V C and Schröer W 2007 *Int. J. Thermophys.* **28** 506
[87] Dittmar H R and Schröer W H 2009 *J. Phys. Chem.* B **113** 1249
[88] Walden P and Centnerszwer M 1903 *Z. Phys. Chem.* **42** 432
[89] Holbrey J D, Reichert W M and Rogers R D 2004 *Dalton Trans.* 2267
[90] Deetlefs M, Hardacre C, Nieuwenhuyzen M, Padua A A H, Sheppard O and Soper A K 2006 *J. Phys. Chem.* B **110** 12055
[91] Qiao B, Krekeler C, Berger R, Site L D and Holm C 2008 *J. Phys. Chem.* B **112** 1743
[92] Japas M L and Levelt Sengers J M H 1990 *J. Phys. Chem.* **94** 5361
[93] Kulinskii V L and Malomuzh N P 2009 *Physica* A **388** 621
[94] Kim Y C 2005 *Phys. Rev.* E **71** 051501
[95] Weiss V C and Schröer W 2008 *J. Stat. Mech.* P04020
[96] Widegren J W and Magee J A 2007 *J. Chem. Eng. Data* **52** 2331
[97] Marsh K N (ed) 1995–2003 *Thermodynamic Properties of Organic Compounds and Their Mixtures* (*Landolt Börnstein New Series* vol IV/8) (Berlin: Springer)
[98] Heintz A, Klasen D and Lehmann J K 2005 *J. Solut. Chem.* **34** 1135
[99] Madelung O (ed) 1991 *Static Dielectric Constants of Pure Liquids and Liquid Mixtures* (*Landolt Börnstein, New Series* vol IV/6) (Berlin: Springer)
[100] Lechner M D 2008 *Static Dielectric Constants of Pure Liquids and Liquid Mixtures* (*Landolt Börnstein, New Series* vol IV/6) (Berlin: Springer)
[101] Crosthwaite J M, Aki S N V, Maginn E J and Brennecke J F 2005 *Fluid Phase Equilib.* **228/229** 303
[102] de Andrade J, Boes E S and Stassen H 2002 *J. Phys. Chem.* B **106** 13344
[103] Zuckerman D M, Fisher M E and Lee B P 1997 *Phys. Rev.* E **56** 6569
[104] Shelley J C and Patey G N 1999 *J. Chem. Phys.* **110** 1633
[105] Hardacre C, Holbrey J D, McMath S E J, Bowro D T and Soper A K 2003 *J. Chem. Phys.* **118** 273
[106] Urahata S M and Ribeiro M C C 2004 *J. Chem. Phys.* **120** 1855
[107] Weast R C (ed) 1963 *Handbook of Chemistry and Physics* 49th edn (Cleveland, OH: CRC Press)
[108] Tokuda H, Hayamizu K, Ishii K, Susan M A B H and Watanabe M 2005 *J. Phys. Chem.* B **109** 6103
[109] Weingärtner H 1989 *Ber. Bunsenges. Phys. Chem.* **93** 1058
[110] Lachwa J, Bento I, Duarte M T, Canongia Lopes J N and Rebelo L P N 2006 *Chem. Commun.* **23** 2445